Master's thesis

NTNU
Norwegian University of Science and Technology
Faculty of Natural Sciences
Department of Materials Science and Engineering

Theresa Nguyen

Electrochemical processes in the $AlCl_3$-urea ionic liquid analogue

Master's thesis in Chemical engineering and biotechnology
Supervisor: Espen Sandnes
Co-supervisor: Christian Rosenkilde
June 2019

NTNU
Norwegian University of
Science and Technology

Theresa Nguyen

Electrochemical processes in the $AlCl_3$-urea ionic liquid analogue

Master's thesis in Chemical engineering and biotechnology
Supervisor: Espen Sandnes
Co-supervisor: Christian Rosenkilde
June 2019

Norwegian University of Science and Technology
Faculty of Natural Sciences
Department of Materials Science and Engineering

NTNU
Norwegian University of
Science and Technology

Acknowledgements

Working with this master thesis have been a journey with both moments of joy and frustration, and would not have been possible without the guidance and help from my two supervisors, Espen Sandnes and Christian Rosenkilde. I want to express my gratitude, first of all, to my main supervisor Espen Sandnes who have been patient and supported me throughout the master project, helping me interpret the experimental data, that for the most time seemed confusing and inexplicable. Further, I want to express my gratitude to my co-supervisor Christian Rosenkilde who gave me tips and ideas to what I could try out in the lab, Geir Martin Haarberg who would find the time to answer any questions, discuss results, and commenting the manuscript. Finally, I want to thank the technical staff Magnus B. Følstad and Anita Storsve, Bartlomiej Gawel that trained me in Raman spectroscopy and Sergey Khromov that trained me in SEM, and the PhD students at the lab who gave tips and tricks to small improvements of the electrochemical setup.

Abstract

Every year, nearly 70 million tons of aluminium is produced worldwide for a wide range of industries, e.g., automotive, electronics, and packaging industries. The material is high in demand due to its unique properties and availability. Primary aluminium is produced through the high-temperature Hall-Héroult process, which is both energy consuming and polluting.

Aluminium can also be deposited from low-temperature melts. Among these, aluminium deposition from an $AlCl_3$-urea ionic liquid analogue has been suggested to be a promising option, due to the availability and low cost of urea. This work has aimed to obtain a general picture of the electrochemical processes on different electrodes in the $AlCl_3$-urea ionic liquid analogue, with and without NaCl. In order to achieve this, $AlCl_3$-urea and $AlCl_3$-urea-NaCl of different compositions have been prepared, and the electrolytes have been investigated with Raman spectroscopy. The information obtained was used in the electrochemical analysis.

Three ionic species was found in the melt, $AlCl_4^-$, $Al_2Cl_7^-$ and $[AlCl_2(urea)_2]^+$. Aluminium deposition occurred at two potentials. First at around $-0.1\,V$ (vs Al) from $Al_2Cl_7^-$ and secondly at around $-1.1\,V$ (vs Al) from $[AlCl_2(urea)_2]^+$. The deposition potential was dependent on the electrolyte composition. At lower $AlCl_3$ content, the deposition shifted to higher cathodic potential. Adding NaCl reduced the cathodic current density because the salt reacted with the electroactive species. It also promoted a gas reaction which was believed to be chlorine evolution. A different anode process, i.e. chloroaluminate intercalation was observed on carbon electrodes. The process was chemically reversible, but at higher anodic potentials, the process led to the disintegration of the electrode.

Sammendrag

Hvert år produseres det nesten 70 millioner tonn aluminium på verdensbasis som blir anvendt i ulike industrier, blant annet transport-, elektronikk- og emballasjeindustrien. Materialet er høyt etterspurt grunnet sine unike egenskaper og tilgjengelighet. Primæraluminium produseres gjennom høytemperaturprosessen Hall-Héroult, som både er energikrevende og forurensende.

Aluminium kan også utvinnes fra lavtemperatursmelter. Blant disse har aluminiumutvinning fra en $AlCl_3$-urea ionisk væske analog blitt foreslått som et lovende alternativ til Hall-Héroult, grunnet tilgjengeligheten av urea og lave kostnader knyttet til stoffet. Målet med dette arbeidet har vært å få et oversiktsbilde av de ulike elektrokjemiske prosessene som forgår på forskjellige elektroder i en $AlCl_3$-urea smelte, med og uten tilsatt NaCl. For å oppnå dette har $AlCl_3$-urea og $AlCl_3$-urea-NaCl med forskjellige sammensetninger blitt fremstilt. Væskene ble undersøkt med Raman spektroskopi og informasjonen ble brukt i den elektrokjemiske analysen.

Tre ioniske komplekser ble funnet, $AlCl_4^-$, $Al_2Cl_7^-$, og $[AlCl_2(urea)_2]^+$. Aluminium ble utfelt ved to potensialer. Først ved ca. $-0.1\,V$ (vs Al) fra $Al_2Cl_7^-$ og deretter ved $-1.1\,V$ (vs Al) fra $[AlCl_2(urea)_2]^+$. Utfellingspotensialet var avhengig av elektrolyttsammensetning. Ved lavere $AlCl_3$ innhold i væsken, flyttet utfellingsreaksjonen til høyere katodiske potensial. Tilsats av NaCl reduserte den katodiske strømtettheten fordi saltet reagerte med de elektroaktive kompleksene. NaCl ledet også til utvikling av en gass, som antakeligvis var klor. En annen anodeprosess, interkalering av "chloroaluminates", ble observert på karbonelektroder. Prosessen var kjemisk reversibel, men ved høyere anodiske potensialer førte prosessen til nedbrytning av elektroden.

List of abbreviations

Table 0.0.1: List of abbreviations

Abbreviation	Explaination
SHE	standard hydrogen electrode
IL	ionic liquid
ILA	ionic liquid analogue
NMA	N-methylacetamide
DMA	N,N-dimethylacetamide
EMII	1-Ethyl-3-methylimidazolium iodide
EMIC	1-Ethyl-3-methylimidazolium chloride
GIC	graphite intercalation compound
MS	mass spectroscopy
NMR	nuclear magnetic resonance
EIS	electrochemical impedance spectroscopy
GC	glassy carbon
Pt	platinum
W	tungsten
OCP	open ciruit potential
IR-drop	potential drop due to the current-resistance relationship
WE	working electrode
CE	counter electrode
RE	reference electrode
SEM	scanning electron microscopy
EDS	Energy Dispersive X-Ray Spectroscopy

Table of Contents

Chapter 1

Introduction

Aluminium is a primary choice of material for a wide range of industries, e.g., automotive, electronics, and packaging industries due to its properties and availability [1]. The resource is the third most abundant element in the earth's crust, and the metal is lightweight, corrosion resistant, easy to recycle, flexible, and has excellent conductivity. Over the last 20 years, the annual average primary production grew 3 % to 4 %, and it is required to continue increasing the production to cover the demand in the years to come.

The conventional method to produce aluminium is through the Hall-Héroult process. Alumina (Al_2O_3) dissolved in a cryolite melt reduces to aluminium at 940 °C-980 °C. This process faces two significant challenges, high energy consumption, and small cell units, leading to high operational and capital costs. Due to the increased awareness about climate changes, pollution from production is also something that needs to be addressed. The aluminium industry is the most polluting metal industry outside Norway because the primary source of energy is coal. So, while the world demands more sustainable production, the rapid development of infrastructure and technology demands for more aluminium. It is, therefore desired to develop a process that is energy-efficient, climate-friendly, and sustainable.

Through the years, several processes have been suggested like the carbothermic reduction of alumina, and electrolysis from chloroaluminate-akali melts [2, 3]. In the carbothermic reduction, alumina reacts with coal in a chemical reaction at 2100 °C:

$$Al_2O_3 + 3\,C = 2\,Al + 3\,CO(g) \tag{1.0.1}$$

Compared to the Hall-Héroult, this process reduces energy consumption with 32 %. However, due to side reactions at temperatures around 2100 °C, the final yield is lowered, making it inferior to the current process. In the end, due to the electrochemical nature of aluminium, most processes have been based on aprotic, non-aqueous solvents or molten salts with aluminium in compound with halides like chloride, sulfide, and nitride. During the 1970s, research on metal deposition from a low-temperature melt became a popular research field. This new class of low-temperature electrolytes was called ionic liquids. They showed considerable potential for deposition of metals with low reduction potentials compared to the standard hydrogen electrode (SHE). Characteristics like low viscosity, high metal salt solubility, high electrochemical and thermal stability, made aluminium deposition from these liquids a promising option. However, other challenges related to production cost hindered the processes from being commercialized.

With the current development of technologies, ionic liquids have become more accessible. In the last decade, a new subclass of ionic liquids called ionic liquid analogues has emerged in the literature. Some of these are cheaper to produce and can be promising for electrowinning of less noble metals. This project is about investigating the possibility of aluminium deposition from an ionic liquid analogue.

1.1 Ionic liquids and analogues

Traditionally, ionic liquids (ILs) have been defined as a composition of salts with a deep depression of the freezing point. Commonly the melting point is below 100 °C [4]. The IL usually consists of large organic cations with low or no symmetry based on quaternary ammonium, sulphonium or phosphonium halides and anions based on Lewis acid metal halides [5]. Figure 1.1.1 shows a selection of the most common components in ILs. The IL is synthesized by the following reaction between the organic halide and metal halide:

$$[\mathrm{Organic}]\mathrm{X} + \mathrm{nMX_m} \rightarrow [\mathrm{Organic}]^+ + [\mathrm{M_nX_{n\times m+1}}]^- \tag{1.1.1}$$

, where X is the halide and M is the metal. The large organic cation prevents efficient packing into a low energy crystal structure, in addition, to weaken and shield the electrostatic forces between the ions. In many cases the molecules also have delocalized charges, further reducing the electrostatic forces. The Lewis acid nature of the metal halide promotes the formation of bonds between the chemicals. These factors together contribute to low melting point and relative high ion mobility. However, even though the electrostatic forces between the ions are weakened, the combination of hydrogen bonding, hydrophobic interactions, and electrostatic forces contribute to low flammability and volatility properties. Depending on the mole ratio between the Lewis acid metal halide and the organic halide, several anion complexes with different Lewis acidity may be formed. This gives ILs the unique ability of adjustable Lewis acidity.

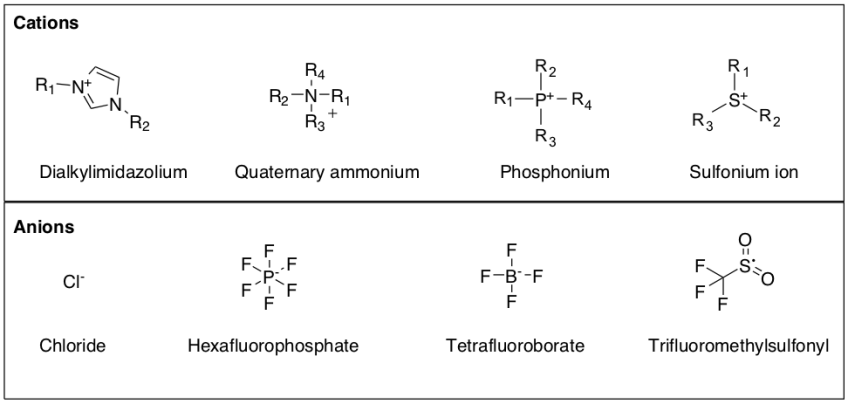

Figure 1.1.1: Common cations and anions found in ionic liquids

Ionic liquid analogues (ILAs) are a subclass of ILs where the quaternary organic halide has been substituted with simple non-ionic species like alcohols and amides. Most of their physicochemical properties are similar to ionic liquids, however, because they can be obtained from non-ionic species, they are not entirely ionic [4]. Usually, the liquid phase of the ILA is generated by self-association through hydrogen bonds. It is believed that strength of the hydrogen

bond donor, i.e. its ability to form hydrogen bonds with the metal halide, determines the melting point. A stronger hydrogen network leads to a lower melting point. The network also prevents ion mobility, which contributes to the high viscosity and low conductivity in ILAs compared to ILs. The introduction of neutral species also contributes to low melt conductivity.

In 2017 Angell et al. successfully created a high Coulombic efficiency battery with the $AlCl_3$-urea ILA as the electrolyte. It was reported that one of the electrode processes was aluminium reduction and oxidation. Considering that urea is cheap, abundant and environment-friendly, and the production of $AlCl_3$ has become more cost-effective, this electrolyte shows potential in an electrowinning process of primary aluminium.

1.2 Aim of the master thesis

The aim of this master thesis is therefore, to obtain a general picture of the electrochemical processes on different electrodes (platinum, carbon, tungsten) in an $AlCl_3$-urea melt with and without NaCl. As part of work, the preparation of $AlCl_3$-urea and $AlCl_3$-urea-NaCl will be examined. The prepared melts will be investigated by Raman spectroscopy to study the different species and their relation to the electrolyte composition. This information will be used in the electrochemical analysis.

Chapter 2

Literature review

2.1 Properties of the chemicals

Aluminium trichloride

$AlCl_3$ is a strong Lewis acid that reacts violently with water, air, strong oxidizing agents, alkali metals, strong bases, and metals. In contact with oxygen and humidity, the following reactions happen:

$$\begin{aligned} AlCl_3 + 3\,H_2O &\longrightarrow HCl + Al(OH)_3 \\ 2\,AlCl_3 + 3\,O_2 &\longrightarrow Al_2O_3 + 3\,Cl_2 \end{aligned} \tag{2.1.1}$$

Urea

Urea has the chemical formula $CO(NH_2)_2$ and reacts exothermically with metal chlorides, strong oxidizing agents, and chlorine. It decomposes at 132-135 °C.

2.2 Speciation

The aluminium chloride - urea system has been reported to form cationic, anionic and neutral species [6, 7, 8, 9]. The formation of anionic aluminium chloride complexes is dependent on the mole ratio of $AlCl_3$ to urea, analogous to IL. Contrary to conventional IL, the aluminium chloride-urea ILA also consists of cationic aluminium complexes of the form $[AlCl_2(urea)_n]^+$. It was first proposed that n = 1,2 by mass spectroscopy [10]. $[AlCl_2(urea)_n]^+$ (n=1) requires bidentate coordination through both N and O, which commonly occurs through the asymmetric splitting of Al_2Cl_6. This has been observed in $AlCl_3$-N-methylacetamide (NMA) and $AlCl_3$-N,N-dimethylacetamide (DMA) and accredited to the inductive effect of the methyl group. Asymmetric splitting is not as common in $AlCl_3$-urea melts, and monodentate coordination is believed to occur more frequently [6, 10].

Through analysis of NMR and Raman spectra, Coleman et al. postulated that urea only forms bond with aluminium through monodentate coordination and the only cationic species formed is the $[AlCl_2(urea)_2]^+$ complex [6]. The urea molecule replaces chloride as a ligand in the

chloroaluminate complex via the oxygen atom and forms the cation [6, 7]. At equimolar mixture, $AlCl_4^-$ and $[AlCl_2(urea)_2]^+$ is formed and a dynamic equilibrium will form between the neutral, cationic and anionic species:

$$2\,AlCl_3 + 2\,urea \longleftrightarrow [AlCl_2(urea)_2]^+ + AlCl_4^- \tag{2.2.1}$$

With the addition of urea or $AlCl_3$ the equilibrium will break. With the excess of urea (x_{AlCl_3}<0.5), the equilibrium shifts to more neutral species and urea will suspend. With the excess of $AlCl_3$, between 1:1 and 2:1 $AlCl_3$:urea, the dimeric species $Al_2Cl_7^-$ forms. Hu et al. proposed that the formation of $Al_2Cl_7^-$ occurs through a reaction between $AlCl_3$ and $AlCl_4^-$.

$$AlCl_3 + AlCl_4^- \longrightarrow Al_2Cl_7^- \tag{2.2.2}$$

Above 2:1 mole ratio, higher order oligomers like $Al_3Cl_{10}^-$ forms. The exact reaction is not known, but these will be in equilibrium with solid $AlCl_3$. In the speciation system, the monomeric species remain in dynamic equilibria with the dimeric species, and this is illustrated in Figure 2.2.1.

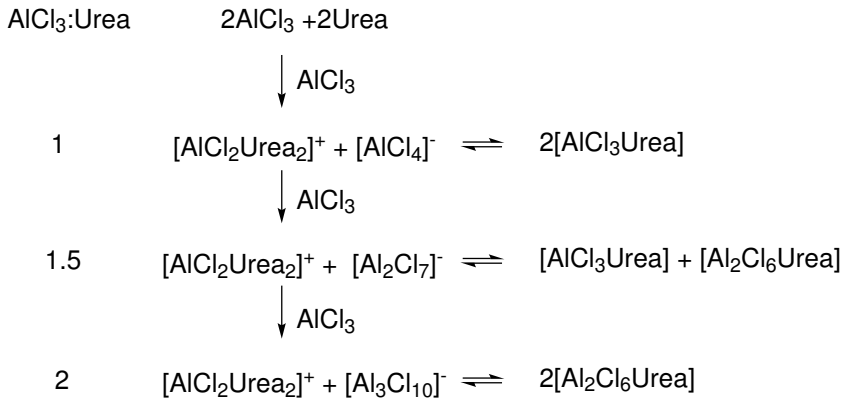

Figure 2.2.1: Equilibrium products of $AlCl_3$-urea system at different mole ratios [6].

Angell et al. did a Raman spectroscopy study of five $AlCl_3$-urea electrolytes in the mole ratio range 1:1-1.5:1 (Figure 2.2.2). Raman spectroscopy showed Raman shifts of $Al_2Cl_7^-$ at 311 cm^{-1} and $AlCl_4^-$ at 347 cm^{-1}. The peak of $Al_2Cl_7^-$ increased with increasing mole ratio of $AlCl_3-$urea, confirming the study of Coleman et al. They also did an Al^{27} NMR analysis, which peaks assignments comply with earlier studies [6, 7, 11]. NMR spectrocopy showed NMR shifts of $AlCl_4^-$ (101.5 ppm), $[AlCl_3(urea)]$ (88.0 ppm), $[AlCl_3(urea)_2]$ (52.7 ppm), $[AlCl_2(urea)_2]^+$ (71.8 ppm) for 1:1 mole ratio, while for the 1.3:1 mole ratio, the region of the spectrum included $AlCl_4^-$, $[AlCl_2(urea)_2]^+$, $Al_2Cl_7^-$.

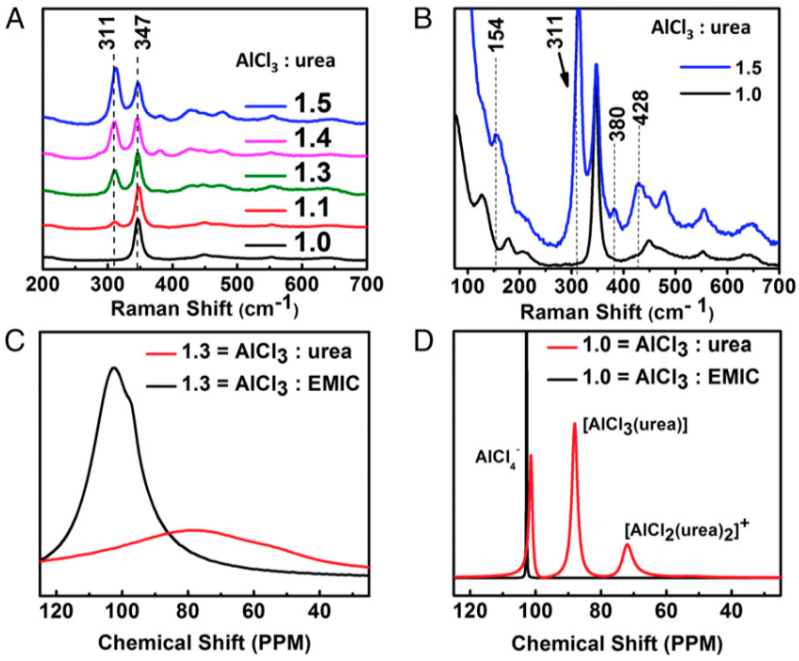

Figure 2.2.2: Figure taken from Angell et al. [12]: Electrolyte speciation study. (A) Raman spectra of $AlCl_3$/urea = 1.0, 1.1, 1.3, 1.4, 1.5 electrolytes, normalized to peak at 347 cm^{-1} ($AlCl_4^-$). (B) Zoom of A to elucidate lower intensity modes of $Al_2Cl_7^-$ (154 cm^{-1}, 310 cm^{-1}, 380 cm^{-1}, 428 cm^{-1}), 1.3, 1.4 electrolytes spectra omitted for clarity. ^{27}Al NMR spectra for (C) $AlCl_3$/urea = 1.3 vs. $AlCl_3$/EMIC = 1.3 and (D) $AlCl_3$/urea = 1.0 vs. $AlCl_3$/EMIC = 1.0. Peak assignments based on the work of Coleman et al. [6].

Abbott et al. assigned the NMR peaks based on MS and their assignment disagrees with Coleman et al. [10]. In later papers, they have not changed their assessment even though it has been demonstrated that MS produces incorrect results for chloroaluminate systems [13]. They assigned δ = 102 ppm to $[AlCl_2(urea)_2]^+$, 88 ppm to $AlCl_4^-$ and 74 ppm to $[AlCl_2(urea)]^+$ [14]. It was proposed that $AlCl_3$ fully dissociates into ion complexes and therefore neutral $AlCl_3$ species does not exist in solution. Based on these results, Abbott et al. proposed that $Al_2Cl_7^-$ does not form in these systems, and the electroactive species are therefore the cationic aluminium complexes. The assignment was supported by several papers working with ionic liquid analogues [15, 16]. The NMR assignments from several papers are presented in table 2.2.1.

Table 2.2.1: Table comparing the reported ^{27}Al NMR assignments.

Author	74 ppm	88 ppm	102 ppm
Abbott, Endres, Fang [10, 15, 16]	$[AlCl_2(urea)]^+$	$AlCl_4^-$	$[AlCl_2(urea)_2]^+$
Coleman, Hu [6, 7]	$[AlCl_2(urea)_2]^+$	$AlCl_3(urea)$	$AlCl_4^-$

The peak intensities from Raman spectroscopy can be used to calculate the relative concentrations of the ionic species in the ILA [17, 18]. The relative concentrations are found by quantitatively measuring the peak intensity (height) of two bands, that each represents a species as a function of mixture composition. The model is shown for $[Al_2Cl_7^-]/[AlCl_4^-]$ with the associated 347 cm^{-2} and 311 cm^{-2} peak recorded by Angell et al. as an example 2.2.3.

$$\frac{I_{347}}{I_{311}} = K\frac{[Al_2Cl_7^-]}{[AlCL_4^-]} \tag{2.2.3}$$

2.2.1 Acidic species present in the ILA

The Lewis acidity of the species in the $AlCl_3$-urea system is to some degree an indicator on which species that are the most reactive and might participate in the aluminium deposition. Abood et al. demonstrated with Friedel Craft experiments that the cationic aluminium species $[AlCl_2(urea)_n]^+$ are more acidic than $Al_2Cl_7^-$ [10]. They compared the $AlCl_3$-EMII alkylation rate in the $AlCl_3$-urea system with the $AlCl_3$-EMII system where $Al_2Cl_7^-$ was the only acidic species. The reaction rate was higher in $AlCl_3$-urea, and this was attributed to the $[AlCl_2(urea)_n]^+$ species.

The $AlCl_4^-$ complex, on the other hand, has been long known to be alkaline and the dominating species in mixtures where x_{AlCl_3}<0.5. Hence these melts are alkaline. The basic nature of $AlCl_4^-$ is attributed to the tetrahedral and symmetric structure, which hinders other molecules from interacting with the Al atom, making the anion stable and very little reactive.

2.3 Limits of the electrochemical window

ILAs are known for their relatively stable and large electrochemical window. The window is, however defined differently depending on the goal of research. Li et al. investigated the electrochemical limits by linear scan voltammetry in a pure urea-acetamide-lithium halide melt [19, 20]. The anodic limit was assigned to the formation of polymeric products. The exact reaction potential was reported to be dependent on the lithium halide (e.g. Cl, Br, F). The cathodic limit was assigned to hydrogen evolution through the breakdown of urea at$-0.8\,V$. The reaction is shown in scheme 2.3.1.

$$NH_2 - CO - NH_2 + e^- \longrightarrow \frac{1}{2}H_2 + NH_2 - CO - NH^- \tag{2.3.1}$$

2.4 Physicochemical properties

The $AlCl_3$-urea melt consists of large ionic species that affect the properties of the liquid. Abbott formulated the hole theory that describes the fluid properties of IL and ILA based on models of ion movements in molten salts [21]. Upon the phase transition between solid and liquid, voids of random size and position emerge due to thermally created fluctuations in local density. The radius of the average sized void $\langle r^2 \rangle$ is dependent on the surface tension of the liquid:

$$4\pi\langle r^2\rangle = 3.5kT/\gamma \tag{2.4.1}$$

where k is the Boltzmann constant, T the absolute temperature and γ is the surface tension of the liquid. The probability to find a hole of radius r in a given liquid is:

$$Pdr = \frac{16}{15\sqrt{\pi}} a^{7/2} r^6 e^{-ar^2} dr \tag{2.4.2}$$

Thus the probability of finding a hole that is large enough to fit an ion is the integration of equation 2.4.2 over all holes that are equal or larger than the ion. These holes are in constant motion. The ionic species move in the melt through adjacent holes (vacancies) that are of equal or greater size. Compared to other conventional liquids, ILA has a high ion radius/hole radius mole ratio [5]. The limited availability of suitably sized holes restricts the ionic motion, and the viscosity is therefore high, while the mass transport is low in these types of room temperature melts.

Overall the conductivity of $AlCl_3$-urea melts has shown to have lower conductivity and higher density than other $AlCl_3$-amide systems [22, 23, 24]. This has been contributed to the lack of asymmetric splitting in this melt due to monodentate coordination. The bidentate coordination favours asymmetric splitting, which results in a higher conversion degree of neutral complexes to ionic complexes. The number of available and unrestricted hydrogen atoms also contributes to fluid properties. Urea has two NH_2 molecules that can donate hydrogen bonds that form a strong hydrogen network through the liquid. This reduces the voids, which in turn increases the density and viscosity of the liquid. Contrary, many other amides, e.g. acetamide, have one of the primary amides substituted with an alkyl group, which is a weak hydrogen bond donor. Increasing the temperature has, however, shown to increase the conductivity of an $AlCl_3-$urea melt, and decrease the viscosity. Liu et al. studied the conductivity, viscosity and density of $AlCl_3-$urea melts at temperatures between 60 100°C [23]. The reported data is given in table 2.4.1. They concluded that the conductivity of $AlCl_3$-urea melt was dependent on the mole ratio $AlCl_3$:urea (speciation) and the molar volume of the $AlCl_3$-urea melt. With increasing temperature, the molar volume increases as the voids in the liquid expands. This increases the number of suitable holes, and conductivity increases.

Table 2.4.1: Density, viscosity and conductivity data for $AlCl_3$-urea melts of various mole ratios [23]

Mole ratio ($AlCl_3$:urea)	60 °C	70 °C	80 °C	90 °C	100 °C
Density [$g\,cm^{-3}$]					
1.2:1	1.5606	1.5522	1.5443	1.5352	1.5275
1.3:1	1.5721	1.5635	1.5551	1.5463	1.5380
1.5:1	1.5921	1.5823	1.5728	1.5624	1.5534
Viscosity [mPa s]					
1.2:1	23.9292	18.2842	14.2663	11.4953	9.5290
1.3:1	24.2543	18.3444	14.3724	11.6215	9.7437
1.5:1	26.8873	20.2734	15.7788	12.7720	10.4479
Conductivity [$ms\,cm^{-1}$]					
1.2:1	4.35	5.49	6.84	8.18	9.76
1.3:1	4.31	5.48	6.75	8.05	9.50
1.5:1	4.11	5.24	6.46	7.63	18.93

2.5 Aluminium deposition in $AlCl_3-$urea ILA

Aluminium deposition in the $AlCl_3-$urea melt has been well documented. There is however, disagreement in the literature about the participating species in aluminium deposition, due to the different views on the speciation of the ILA system. Abbott et al. proposed that the deposition occurs with cationic species through reaction 2.5.1 [14]. Figure 2.5.1 shows the voltammograms recorded at different mole ratios by the research group. They proposed that the deposition potential shifts to higher cathodic potential in equimolar electrolytes due to different electrolyte speciation.

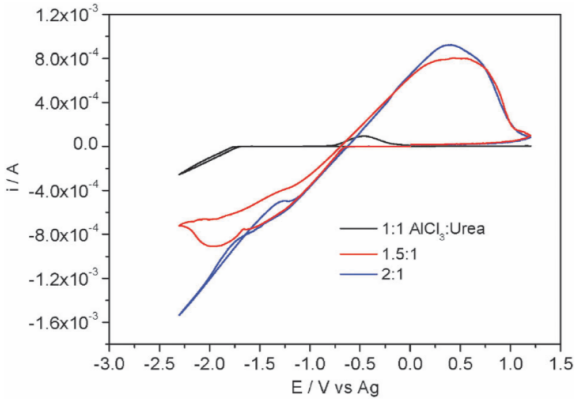

Figure 2.5.1: Figure taken from Abbott et al. [14]. Cyclic voltammetry of various $AlCl_3$-urea electrolytes as function of composition on a GC disc electrode.

Coleman et al. observed that Al deposition from $AlCl_3$-DMA melts occurred at a more negative potential than in similar chloroaluminate IL systems (i.e. $AlCl_3$-EMIC). It was believed that the monomeric cationic aluminium species, rather than the $Al_2Cl_7^-$ species was reduced.

$$2\,[AlCl_2(urea)_2]^+ + 3\,e^- \longrightarrow Al + AlCl_4^- + 4\,(urea) \tag{2.5.1}$$

Reduction of $Al_2Cl_7^-$ is well documented in conventional chloroaluminate IL systems and occurs through equation 2.5.2.

$$4\,Al_2Cl_7^- + 3\,e^- \longrightarrow Al + 7AlCl_4^- \tag{2.5.2}$$

The deposition process requires a nucleation overpotential to initiate and follows a 3-D instantaneous nucleation model at short time scales before it starts to deviate from the model at longer timescales [14, 20]. Li et al. describe the possible Al nucleation process by studying results from chronoamperometry [20]. A nucleation overpotential is required for the deposition process to initiate. It contributes to the nucleation and growth of nuclei. After a double layer charging, the nucleation and growth of nuclei contribute to increasing the Faradaic currents. The increasing current eventually reaches a plateau due to the discrete diffusion zones of individual growing nuclei's overlap and grow together. After t_m, where the current density is at its maximum value, the current density decreases due to the growing diffusion layer thickness.

The $AlCl_3$-urea system has a different growth mechanism from other ionic liquids, most likely due to the participation of $[AlCl_2(urea)_2]^+$ species in the deposition process. $AlCl_4^-$ which has

been reported to be an electroactive species in chloroaluminate molten salts, is not electroactive in this ILA [12, 14]. The morphology and appearance of the deposit dependents on several factors among others, electrode material, temperature, potential, mole ratio, stirring rate, additives and time [10, 25, 20, 14, 26]. The crystal structure, on the other hand, seems to be unaffected. The following sections will elaborate on the different factors affecting aluminium deposition.

2.5.1 The effect of temperature

The temperature influence the conductivity, viscosity and ion mobility of the $AlCl_3$-urea melt. These factors affect the aluminium deposition rate and the surface morphology, i.e. the particle size and roughness of the deposit [25]. At low temperatures up to 40 °C the deposit is dense and brighter due to smaller particles, while at temperatures above 40 °C the surface is uneven and contains cracks and holes, giving a dull grey appearance. The adhering ability of the deposit to the substrate increase until 60 °C, where it decreases.

2.5.2 Electrode materials

Aluminium deposition on a foreign substrate requires a nucleation overpotential to occur. Also, different electrode materials can react with both the electrolyte and aluminium deposit through various processes. This might give unwanted products that hinder the deposition process or alloying products that reduce the purity of the deposit. The substrate material might also affect the deposition rate. Some of the most common working electrodes for investigation of aluminium deposition in ionic liquids and analogues are platinum, glassy carbon and tungsten [14, 20, 27]. For aluminium electrolysis, copper is a popular choice [10, 25].

Platinum is a sturdy and corrosion resistant material. The disadvantage of platinum is that it forms alloying compounds with aluminium (Appendix B.0.1). Platinum can also form compounds with chlorides [28]. Using platinum as a working electrode in this $AlCl_3$-urea melt for aluminium deposition/stripping might therefore, give unwanted side reactions.

Glassy carbon (GC) is an inert electrode material, which does not form any known compounds with aluminium. It is therefore, a good material for electrochemical analysis. The disadvantage of GC is that aluminium has poor adhesion ability to the material.

Tungsten is an inert electrode material in chloroaluminate melts. It may form several alloys with aluminium (Appendix B.0.2) and compounds with chloride [29].

Copper has been reported to be a suitable cathode material for aluminium deposition. The aluminium deposit adheres well to copper. It is however, not a good material for electrochemical analysis with, e.g. cyclic voltammetry due to the close oxidation potential to aluminium oxidation. This results in a possibility of copper dissolution and introduction of copper impurities that can deposit with aluminium, decreasing the deposit purity.

2.5.3 The effect of adding alkali chlorides

In this study, sodium chloride was added to the $AlCl_3$-urea melt, and the effect was investigated as an additive to increase the conductivity and improve the overall aluminium deposition process. Comprehensive studies have been done on the speciation of aluminium in $AlCl_3-NaCl$ melts. The behaviour of $AlCl_3$ is similar in this system to the $AlCl_3$-urea melt. Anodic aluminium oligomers form according to the acidity of the $AlCl_3-NaCl$ melt. In other words, with excess $AlCl_3$, higher order aluminium complexes like $Al_2Cl_7^-$ will be present in the liquid. Scheme 2.5.3 shows the reaction path of equimolar $AlCl_3-NaCl$

$$AlCl_3 + NaCl \longrightarrow AlCl_4^- + Na^+ \tag{2.5.3}$$

An acid-base equilibrium is established between the acidic species $Al_2Cl_7^-$ and the basic species $AlCl_4^-$ at 175 °C, where the equilibrium constant under these conditions was determined to be K = 1.06×10^{-7} [30].

$$2\,AlCl_4^- \longleftrightarrow Al_2Cl_7^- + Cl^- \tag{2.5.4}$$

In conventional IL, the NaCl acts as a buffer due to the acid-base equilibrium, and it is therefore, easier to produce a neutral melt by adding NaCl until neutrality is achieved than preparing an equimolar melt by combining the weighted portions of the chemicals [31].

Abood et al. proposed an acid-base equilibrium in $AlCl_3$-urea melts with alkali metals, analogous to the one found in the $AlCl_3$-NaCl system [32]:

$$[AlCl_2(urea)_2]^+ + 2\,Cl^- \longrightarrow AlCl_4^- + 2\,urea \tag{2.5.5}$$

Instead of the $Al_2Cl_7^-$ complex, the cationic aluminium complex participates in the equilibrium. A Lewis acid-base titration with chloride ions in an $AlCl_3$-urea toluene/benzene electrolyte demonstrated this. The acidic species form coordination complexes with the aromatic rings. Melts of mole ratio 2:1 and 1.5:1 $AlCl_3$-urea were tested. The result from the paper is however, arguably because it does not take into consideration that the Lewis acid $Al_2Cl_7^-$ also exists at these mole ratios and will participate in the reaction.

Abbott et al. studied the effect of adding LiCl to $AlCl_3$-urea. It is believed to react with the cationic complex to form a Lewis basic complex [14]. By the addition of 1 wt% LiCl to an equimolar $AlCl_3$:urea electrolyte, the aluminium deposition/stripping current was significantly reduced. Because the equimolar does not contain the acidic anion, LiCl reacted with the cationic species $[AlCl_2(urea)_n]^+$, proving that the species is reduced to aluminium at equimolar melts.

$$[AlCl_2(urea)_n]^+AlCl_4^- + 2\,LiCl \longleftrightarrow 2\,[Li(urea)_nAlCl_4] \tag{2.5.6}$$

Abbott et al. further investigated the effect of adding LiCl [9]. Li^+ is a small and strongly polarizing cation, acting as a strong Lewis acid, the cation will lower the T_d symmetry of $AlCl_4^-$. This promotes the dissociation of $AlCl_4^-$ to $AlCl_3$ and Cl^-. The second explanation is that the Li cation is present at the cathode surface and promotes the adsorption of $AlCl_4^-$ at the electrode surface.

2.6 Possible anode processes

Most research done on the $AlCl_3$-urea melt for commercial purposes has proposed the process for electroplating. In electroplating, the anode is usually the metal that is going to be plated. Hence the anode processes in this melt have not been researched to such an extent. It was not until recently that two articles (Jiao et al. [8] and Angell et al. [12]) reported another anode process in $AlCl_3$-urea batteries where the negative electrode (cathode during charging) was graphite and aluminium was the positive electrode (anode during charging). A chloroaluminate intercalation process was reported to occur on the positive electrode. In similar $AlCl_3$-systems, the anode process has been well documented. Chloroaluminate intercalation was also reported in $AlCl_3$-EMIC batteries were the positive electrode was graphite [33, 34]. In $AlCl_3$-NaCl melts, three anode processes can occur depending on the electrode material, chloroaluminate intercalation, chlorine evolution and loosely held chlorine absorption on the active electrode site [3, 35, 36, 37].

2.6.1 Chloroaluminate intercalation

Chloroaluminate intercalation/deintercalation occurs in porous carbon materials like graphite due to the hexagonal ABAB stackings structure of graphene sheets, meaning that they can accommodate intercalating species between the layers [38]. In chloroaluminate IL and ILA, anions in the form $Al_xCl_y^-$ diffuse into the graphite layers and form Graphite Intercalation Compounds (GIC) as shown in Equation 2.6.1. Lin et al. demonstrated that the main intercalation anion is $AlCl_4^-$ in the $AlCl_3$-EMIC battery [34]. The graphite electrode can expand by 50 fold due to the intercalation process owing to the weak van der Waals bondings between the graphite layers.

The process is highly disordered at the beginning of the process, but with an increasing amount of $AlCl_4^-$ intercalating into the graphite, the intercalation evolves into highly ordered, coordinated stages, aligning themselves into stage 3 GIC [39]. DTF studies showed that $AlCl_4^-$ is distorted and flattened due to the pressure from the graphite structure when it intercalates. Angell et al. assumingly observed stage 2 GIC at the fully charged state of the $AlCl_3$-urea battery by in-situ Raman spectroscopy [12]. On the other hand, it is claimed by Pan et al. that stage 4 GIC is the most stable in $AlCl_3$-EMIC [39]. Stage 3 is observed at temperatures at $-10\,^{\circ}C$. It is however a metastable system and is kinetically unstable at room temperature.

The intercalation process is chemically irreversible, causing changes to the graphite structure. During the process, the electrode expands and shrinks, and with continuous cycling, this leads to cracks on the surface and changes of the surface area. Also, some species fail to deintercalate and are trapped in the graphite. Due to the relatively large size of the anion, the diffusion of the anion through the graphite is slow, and the anode process is therefore the rate controlling [40]. The intercalation process occurs between 1.6 V and 2.14 V and the deintercalation process occurs between 1.97 V and 1.3 V (vs Al) [12].

$$AlCl_4^- + C_n \longleftrightarrow C_n[AlCl_4]^- + e^- \tag{2.6.1}$$

In $AlCl_3$-NaCl melts, the intercalation/deintercalation process requires a presence of chlorine gas and ceases when the gas is depleted [41]. Analogous to the IL and ILA melt, the interca-

lation/deintercalation reaction is overall reversible, however with continuous cycling swelling and disintegration of the graphite electrode will occur. The process is dominating at room temperature. However at elevated temperature, the chlorine evolution process is dominating. At higher temperature the produced chlorine gas escapes, the electrode surface quicker, leading to less chlorine assisting the intercalation process.

2.6.2 Chlorine evolution

Mohandas et al. reported that chlorine evolution occurs in $AlCl_3$-NaCl melts when the working electrode is a compact electrode material like compact graphite, glassy carbon and metals. The active species in chlorine evolution are Cl^- and $AlCl_4{}^-$. The Cl_2/Cl^- reaction shown in Equation (2.6.2) occurs at lower anodic potential and the equilibrium potential is reported to be 2.15 V (vs Al) at 175 °C and 1 atm. Chlorine evolution from $AlCl_4{}^-$ shown in Equation (2.6.3) occurs at higher anodic potentials due to the stability of the chloroaluminate complex. The equilibrium potential is reported as 2.7 V (vs Al) at 175 °C and 1 atm. Figure 2.6.1a shows a cylic voltammogram of a NaCl saturated $AlCl_3-$NaCl melt on a tungsten electrode. The onset current at (a) corresponds to the chlorine evolution from Cl^-. At higher potentials (b) the chlorine evolution from $AlCl_4{}^-$ starts dominating.

$$2\,Cl^- \longleftrightarrow Cl_2 + 2\,e \tag{2.6.2}$$

$$4\,AlCl_4{}^- \longleftrightarrow 2\,Al_2Cl_7{}^- + Cl_2 + 2\,e^- \tag{2.6.3}$$

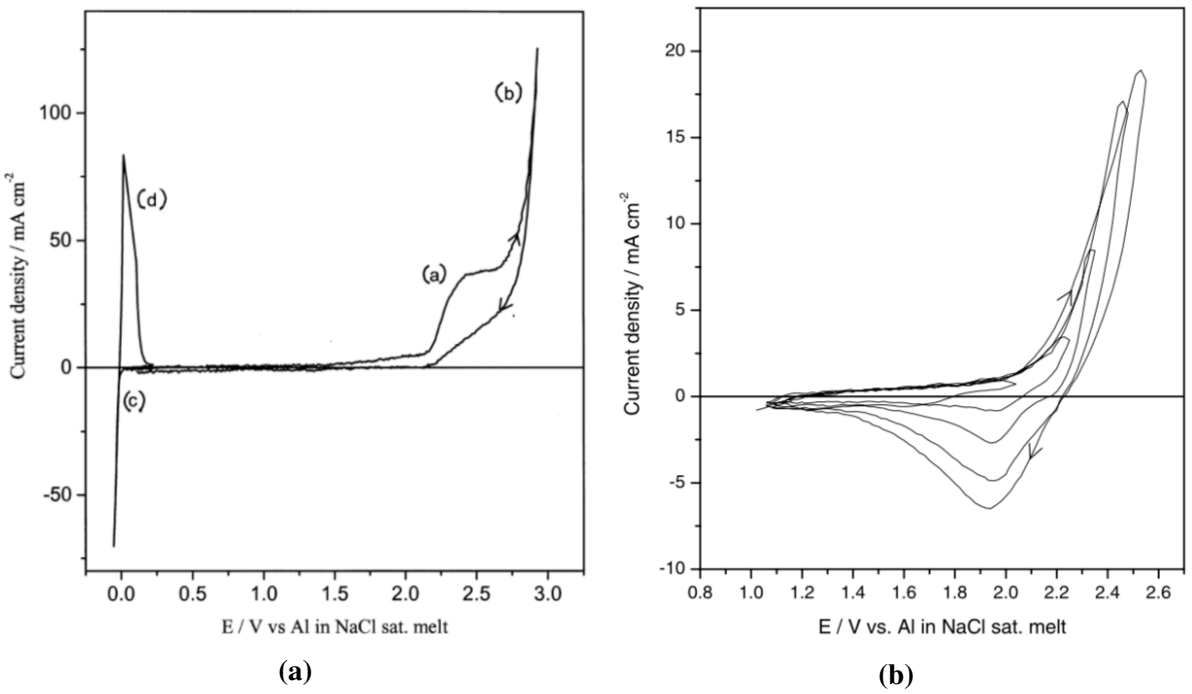

Figure 2.6.1: Figure taken from Mohandas et. al [35]. Cyclic voltammogram of the NaCl saturated $NaAlCl_4$ melt on (a) W (0.008 cm^2) and (b) graphite rod (0.5 cm^2)

The standard potential (vs Al) reported for the Cl^-/Cl_2 couple was 2.15 V while the $AlCl_4{}^-/Cl_2$ was reported to happen at even higher potentials [36]. The same acid/base equilibrium was reported for aluminum chloride based ionic liquids [42, 43, 44]. Chlorine evolution was reported to happen at around 2.7 V through the $AlCl_4{}^-/Cl_2$ reaction [44]. Studies of $AlCl_3-$amide ILAs have not mentioned the acid-base equilibrium [6, 7, 8]. However, these studies have mainly used ^{27}Al-NMR and Raman spectroscopy to investigate the aluminium speciations of the $AlCl_3-$amide system. Thus the Cl^- might have been lost or is invisible in the spectra.

2.6.3 Loosely held chlorine on graphite surface

For room temperature $AlCl_3$-EMIC system, the intercalation process does not proceed to stage 3 GIC at higher anodic potential, but an irreversible process starts at 2.5 V (vs Al) [39]. X-ray spectroscopy has shown that this process is an absorption process of chlorine to graphite. Radical chlorine is bonded to graphite as Cl-C bonds at weak and imperfect areas like edges, cracks and defects. The phenomenon was not observed in the bulk of graphite flakes. A similar process was also observed in AlCl3-NaCl systems, but only for graphite powders [35]. Mohandas et al. suggested that the C-Cl bonds arise through a redox process:

$$C_x + Cl^- \longleftrightarrow C_x - Cl + e^- \tag{2.6.4}$$

2.6.4 Dissolution of aluminium

The number of available suitable ligands limits the dissolution of aluminium [14]. In ionic liquids with free chlorides like the $AlCl_3$-EMIC melt the dissolution proceeds through the following reaction:

$$Al^{3+} + 7\,AlCl_4{}^- \longleftrightarrow 4\,Al_2Cl_7{}^- \tag{2.6.5}$$

There is a lack of chlorine ligands in the $AlCl_3-$urea melt, and the aluminium dissolution likely occurs with urea instead:

$$Al^{3+} + AlCl_4{}^- + 4\text{urea} \longleftrightarrow 2\,[AlCl_2(\text{urea})_2]^+ \tag{2.6.6}$$

Chapter 3

Methodology

3.1 Electrochemical impedance spectroscopy

Electrochemical impedance spectroscopy is a technique that measures the overall impedance of a system. Impedance is the frequency dependent resistance. Every mechanism/component that is involved in the electrochemical process in a cell, e.g. mass transport, double layer capacitance, and solution resistance are contributing to the total potential drop of the cell. While solution resistance is an ohmic and innate property of the cell, non-ohmic resistances like double layer capacitance and charge transfer resistance are frequency dependent. Each component has a characteristic dependence on the frequency, and by investigating it, the contribution of each component to the electrochemical process can be mapped, and the kinetics can be derived. A small amplitude AC voltage is applied on top of the DC potential to an electrochemical system at steady state, and the current response is measured. The AC voltage is applied with various frequencies. Usually, the measurement starts at high frequencies and decrease towards low frequencies. The responding impedance is, therefore defined as:

[45].

$$Z(f) = \frac{E(t)}{i(t)} \tag{3.1.1}$$

where Z is the impedance, E the potential and i the current density. At low frequencies most of the components can follow the perturbation, however with higher frequencies, several components will struggle to keep up. The component responds with a smaller amplitude and increased phase shift until a frequency is reached where they stop responding. The ohmic resistance will always be present because it is not dependent on the frequency. As a result, the solution resistance can be read directly from the measurements at high frequencies where no other processes occur.

$$Z_{\mathrm{R}} = R_s \tag{3.1.2}$$

3.2 Voltammetry

Voltammetry is a technique for studying the electrochemical properties of a system. It involves applying a voltage or series of voltages to a cell and measure the responding current through the working electrode. The variation of the potential is usually time-dependent.

3.2.1 Cyclic voltammetry

In cyclic voltammetry, the potential applied is varied linearly within a set potential range according to a triangular waveform (Figure 3.2.1a). In a typical experiment, the potential is swept to the first limit E_1 from the starting potential E_i. After reaching E_1, the direction of the sweep is reversed, and the electrode potential is swept to the other limit E_2 [46]. The potential is thus described by:

$$E(t) = E_i \pm vt \tag{3.2.1}$$

where v is the scan rate [v/s] that determines the variation speed of the potential. The resulting current response is then plotted as function of potential as shown in Figure 3.2.1b. The plot is called a voltammogram.

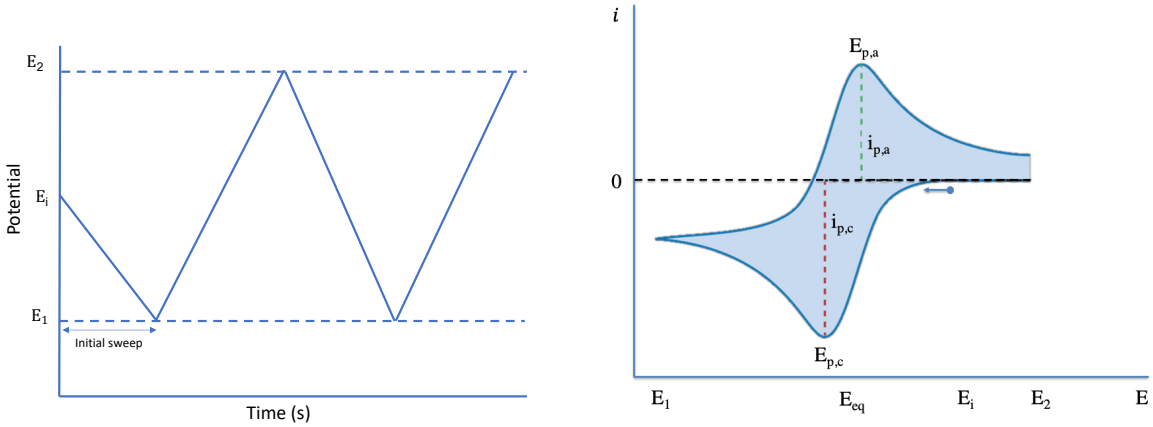

(a) Cyclic potential sweep

(b) Resulting cyclic voltammogram

Figure 3.2.1

3.2.2 Metal deposition/stripping

Formation of a nucleus is the first step of metal deposition on a foreign substrate. The formation of a stable nucleus with a critical radius:

$$r_c = \frac{-2M\gamma}{nF\eta\rho} \tag{3.2.2}$$

is associated with a critical free energy of formation:

$$\Delta G_c = \frac{16\pi M^2 \gamma^3}{3\rho^2 n^2 F^2 \eta^2} \tag{3.2.3}$$

, where γ is the surface tension, M is the molecular weight, ρ is the density of the deposit, n is the number of moles of electrons transferred, F is Faradays number, and η is the overpotential. The deposition of metal on a foreign substrate is therefore associated with a nucleation overpotential. Figure 3.2.2 shows a schematic cyclic voltammogram of metal deposition/stripping that exhibits this behaviour. On the forward sweep, a layer of metal is deposited on a foreign material. Due to the additional energy requirement related to nucleation, the reduction reaction occurs at a cathodic overpotential. However on the reverse sweep, metal will deposit on metal, and the deposition rate is higher. This leads to the characteristic crossover curve for voltammograms describing metal deposition/stripping. The deposit reaction continues until the equilibrium potential is reached, where the stripping reaction starts. The stripping curve is sharp and symmetrical because the oxidizing metal is available on the electrode. The stripping reaction is therefore independent of transport mechanisms. Usually, the nucleation overpotential is larger on the first scan than on the following scans. This is because the metal is not adequately removed during the anodic sweep, leaving nucleation sites for the consecutive sweeps.

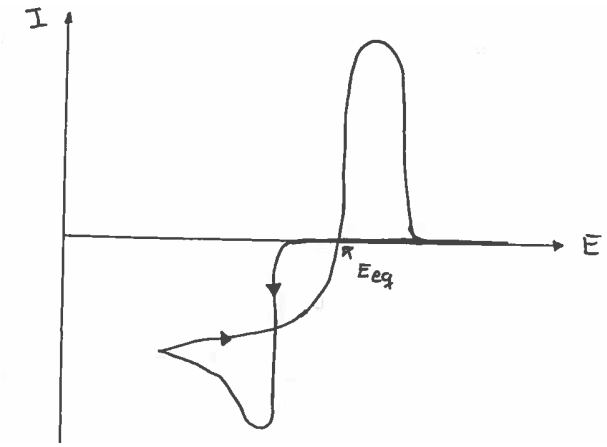

Figure 3.2.2: Schematic cyclic voltammogram of metal deposition /stripping exhibiting nucleation overpotential. Adapted from Instrumental methods in electrochemistry Southampton p.21 [45].

The theoretical mass of deposited aluminium can be calculated through Faradays law:

$$m_{\mathrm{Al}}^{\mathrm{th}} = \frac{i\mathrm{At}}{nFM_{\mathrm{Al}}} \tag{3.2.4}$$

where i is current density, A is area, z is the number of electrons required to reduce one Al^{3+} to aluminium metal and M_{Al} is the molar mass of aluminium.

3.3 IR-drop challenges in relation to electrochemical measurements

When there is a current flowing through an electrolyte, there will always be a voltage drop corresponding to Ohm's law:

$$E = R_u I \tag{3.3.1}$$

, where E is the voltage drop, R_u the uncompensated resistance and I is the current flowing through the cell. Several factors can contribute to the uncompensated resistance R_u. This includes the resistivity of the electrolyte, geometry and size of the electrode, and the resistivity from the electrical conductors connecting the cell to the potentiostat. Normally it is possible to change the cell design to minimize the contribution from conductors and electrodes. This leaves the electrolyte resistance, which is harder to avoid and in most cases, R_u is approximately R_s:

$$R_u \approx R_s \tag{3.3.2}$$

The solution resistance arises due to transport limitations of charge carriers in a solution. Electrical current is dependent on ions as charge carriers to flow from one electrode to the other, through the electrolyte. Electrolytes with high viscosity or few charge carriers will have low conductivity and a high voltage drop.

In a three-electrode cell, the potential is measured between the working and the reference electrode. For a voltammetric experiment, the true potential is then [47]:

$$E = E_i \pm vt - IR_s \tag{3.3.3}$$

where E_i is the start potential. If the applied potential from the potentiostat is $E' = E_i + vt$, then we have the following relationship:

$$\frac{dE}{dt} = \frac{dE'}{dt} - R_s \frac{dI}{dt} \tag{3.3.4}$$

As a faradaic current starts to flow, the true electrode potential will change less than what is recorded by the potentiostat. The opposite will occur when the current has reached the maximum value and is declining. This result in distortion and shifting of the peaks in a very similar manner to slow charge transfer kinetics. Consequently, unknown IR-drop might be misleading in the interpretation of the voltammogram.

3.4 Electrical conductivity

Electrical conductivity is an important physical property that is closely related to several other electrolyte properties like viscosity, mobility and diffusivity [48]. It can be calculated from a set of cell parameters with the following equation:

$$\kappa = \frac{1}{\mathrm{R}_s}\frac{l}{\mathrm{A}} = K_{\text{cell}}\frac{1}{\mathrm{R}_s} \tag{3.4.1}$$

where R is the electrolyte resistance, l is the effective length of the current path, A the cross-section of the current path and K the cell constant. The conductivity can give information about the total amount of ions in the electrolyte.

The conductivity as a function of the temperature follows an Arrhenius relationship [49].

$$\kappa = \kappa_0 \exp(-E_a/kT)/K_{\text{cell}} \tag{3.4.2}$$

, where κ_0 is the preexponential factor and k is the Boltzmann's constant ($8.61733326214\dot{5}10^{-5}$ $\mathrm{m^2\,kg\,s^{-2}\,K^{-1}}$), E_a the activation energy of conduction, and T is the absolute temperature.

3.5 Raman spectrocopy

Raman spectroscopy is a technique that analyses inelastic scattering of monochromatic light to gain qualitative and quantitative information of a sample [50]. The sample is radiated with a monochromatic light source with a wavelength of v_o. This induces an electric dipole moment to the molecules, making them vibrate and send out light with a characteristic wavelength v_m which depends on the molecular symmetry. The new vibrational state of the molecule is called a virtual level. As the molecule drop to ground state, it emits light of a particular wavelength. The light is inelastically scattered if the wavelength has changed. This phenomenon is called the Raman effect and involves a change in dipole moment of the molecule as the light hits and scatter. This requires that the molecule has modes without inversion centres, meaning that they have anti-symmetric modes. As mentioned, oscillating dipoles emits light of different wavelengths that depends on the molecular symmetry. Three cases of scattering are possible:

1. Rayleigh scattering: Elastic scattering of light because the molecule does not have a change in dipole moment, $v_o = v_m$.

2. Stoke scattering: Inelastic scattering of light when a Raman active molecule changes dipole moment. Because the molecule is in its vibrational ground state some energy is required to change the dipole moment and the scattered light has a higher wavelength than the incoming light, $v_o - v_m$

3. Anti-stoke scattering: Inelastic scattering as above, however the molecule starts at an excited state and the molecules emits energy when it scatters light. The scattered light has therefore, a lower wavelength than the incoming light, $v_m - v_o$

The scattering light creates a spectrum that is unique for each chemical compound, making it possible to use the technique to identify an unknown sample. Figure 3.5.1 illustrates the different cases of scattering.

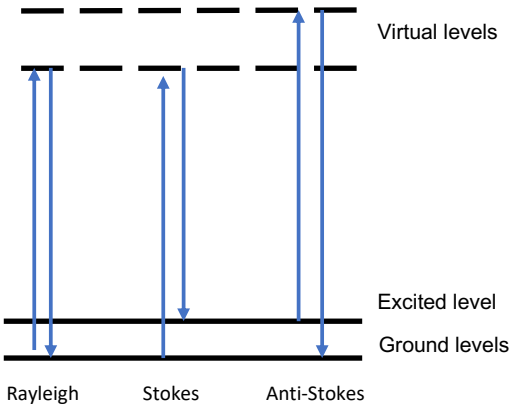

Figure 3.5.1: Illustration of the different scattering modes in Raman spectroscopy

3.6 Scanning electron microscopy

An electron beam adjusted by electromagnetic lenses and apertures that hits a sample in vacuum gives rise to several electron-specimen interactions, as seen in Figure 3.6.1. These interactions can be used to create high magnified resolution images of the specimen. One of the most investigated electron-specimen interactions is secondary electrons (SE). SE are generated from inelastic scattering of the incident electron beam by the electrons in the sample. The probability of a generated SE leaving the sample is based on the topography of the specimen. Increased local curvature makes it easier for the SE to leave because the travel length out of the sample is shorter. On flat surfaces, the SE needs to travel the electron penetration depth. Another signal that is common to investigate is characteristic x-rays that are formed from electron transition between energy levels. The energy from x-rays depends on the atom number and is unique for every element. It can therefore, provide information about the sample composition. The technique is called energy-dispersive X-ray spectroscopy (EDS) and is usually combined with SEM because they both use an electron beam. In EDS, the electron beam is used to promote the electron transitions.

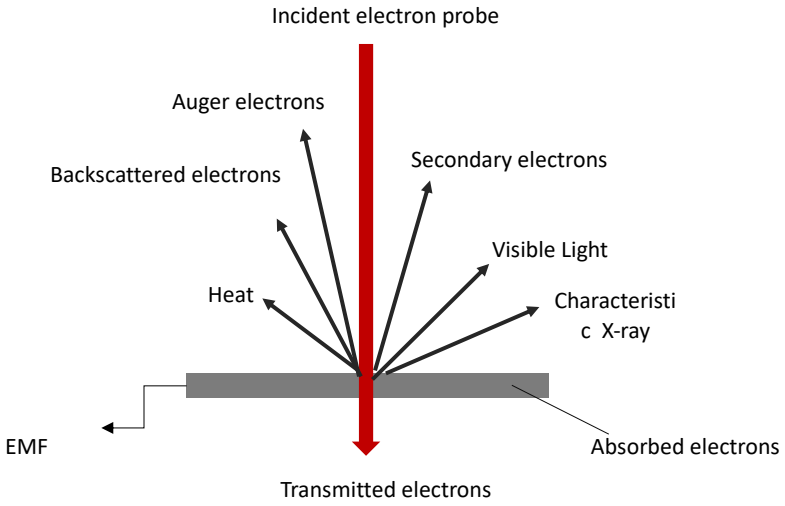

Figure 3.6.1: Overview over the electron-speciemen interaction in SEM. Adapted from Hjelen. J [51].

Chapter 4

Experimental work

4.1 Chemicals

The following chemicals in table 4.1.1 were used to make the electrolytes.

Table 4.1.1: Table over the chemicals in this study, their purity and size.

Chemical	Manufacturer	purity	Size
Urea	Merck	99 %	fine
$AlCl_3$	VWR	99 %	coarse
NaCl	Merck	99.5 %	fine

4.2 Preparation of the electrolyte

$AlCl_3$-urea and $AlCl_3$-urea-NaCl electrolytes of the compositions shown in Table 4.2.1 were prepared. They were prepared in a glove box to avoid degradation of $AlCl_3$ due to its reactivity towards humidity and oxygen. All equipment and urea were thoroughly dried before they were transferred into the glove box. Urea was vacuum dried at 80 °C for 12 h. The equipment was dried for at least 4 hours.

In the glove box, $AlCl_3$ was ground into a fine powder. Urea and $AlCl_3$ were introduced in small amounts and mixed slowly together to avoid violent reactions between $AlCl_3$ and urea. As a liquid began to form, the mixture became less reactive, and urea and aluminium chloride was added in larger amounts and stirred together at a higher speed. The mixture was then heated to 80 °C and stirred for 1 hour to dissolve any remaining solids. NaCl was added at this step and mixed until it was dissolved.

Table 4.2.1: Mole ratio of the electrolytes prepared.

Electrolyte	Mole ratio
$AlCl_3$-urea	1.0:1
	1.3:1
	1.5:1
$AlCl_3$-urea-NaCl	1.5:1:0.25
	1.5:1:0.35
	1.5:1:0.5

4.3 Raman spectroscopy

The speciation of the electrolytes was investigated with the Raman microscope WITec alpha300R. Samples were prepared in the glove box. A drop of the electrolyte was placed on an object glass and covered with a coverslip. The sample was then transferred to the Raman microscope and examined. Spectra were acquired for several positions of the sample and settings were tested to find the one giving the most reproducible results. The final settings that were used for the Raman spectra presented in this report are shown in Table 4.3.1.

Table 4.3.1: Raman microscope settings for data sampling.

Setting	Value
Objective lens	50 x
Laser power	50 kV
Integration time	20 s
Accumulation	5 spectra

Data processing

The acquired spectra were post-processed to make them easier to compare. Background subtraction and the Savitzky-Golay algorithm was applied to smooth the spectra and reduce the noise. The spectra were normalized around the strongest $AlCl_4^-$ peak to make them comparable. The relative concentrations of the ions in solution were found by using equation 2.2.3, where K, the experiment factor, is 87.2 ± 0.02 and using the rules for charge neutrality [12, 17].

4.4 The electrochemical cell

The electrochemical cell used in this work had to satisfy several requirements:

- Fit a three-electrode system with a working electrode (WE), a counter electrode (CE) and a reference electrode (RE)
- Have a small volume because the preparation of the electrolyte was time-consuming and tedious.
- Protect the electrolyte from the humid atmosphere.
- The reference electrode should be relatively constant in melts with different composition and species in solution.
- The distance between the reference and working electrode should be as small as possible to reduce the IR-drop between the electrodes.

Two cell setups were made that each satisfied some of the requirements. These are shown in Figures 4.4.1a and 4.4.1b.

Figure 4.4.1b shows the setup that was used for electrochemical comparison studies of different electrolyte compositions. The reference electrode was composed of an Al wire in a compartment with an 1.5:1 $AlCl_3$:urea melt. It was in contact with the electrolyte through a glass frit. The electrodes were held in place with o-rings and plastic lids.

The setup in Figure 4.4.1a was dedicated to all other electrochemical analysis. The cell container was a glass sample vial, and the lid was adapted to an electrode holder. The lid also served as protection against the humid atmosphere.

(a) **(b)**

Figure 4.4.1: Cell setup for the different electrodes. (a) Setup for analysis (b) Setup for comparing electrolytes.

4.5 Preparation of the electrodes

Table 4.5.1 shows an overview over the electrode materials. Earlier, the author found that glassy carbon worked well for cyclic voltammetry measurements. It has therefore been the main working electrode material. Several electrode setups were tested to reduce the problem with high solution resistance, i.e. the limitation of the potentiostat to IR compensate at different current ranges.

Table 4.5.1: Table over materials used for the electrodes.

Material	Electrode	Type	Manufacturer	Purity	active WE area
Copper	WE	Foil	Alfa Aesar	99.99 %	0.5 cm^2
Glassy carbon	WE	Rod	-	-	0.03 cm^2
"	"	"	"	"	0.2 cm^2
"	"	"	"	"	0.8 cm^2
Graphite	WE	Rod	Alfa Aesar	99%	0.6 cm^2
"	"	"	"	"	0.94 cm^2
Tungsten	WE	Wire	-	-	0.01 cm^2
Platinum	WE	Sheet	K.A. Rasmussen	99.99%	2 cm^2
1080 Al alloy	WE, CE, RE	Sheet	-	99.8 %	1 cm^2
Aluminium	CE, RE	rod	Merck	99.9998 %	-

Glassy carbon and graphite

Two electrode setups were tested for glassy carbon and graphite. Figures 4.4.1a and 4.4.1b shows the electrode setups. The electrode setup in Figure 4.4.1a was used for electrochemical measurements with temperature and the investigation of anode processes. A cylinder section of the rod was defined as the active area. For the setup electrode setup, the circular cross section of the rod was defined as the active area (Figure 4.4.1b).

The cross-section setup was abraded with Si grit paper of 800, 1000, 2000 roughness and then polished with 0.3 µm alumina paste to obtain a smooth surface. The surface was abraded/polished with circular movements, following the number eight pattern. After the polishing, the rod was cleaned with distilled water, ethanol, acetone and left to dry. The final step was to wrap the rod with Teflon tape, leaving the decided electrode area and the upper part of the rod uncovered (see 4.4.1a). Before the experiment, the glassy carbon electrode was dried in an oven at 120 °C for at least 10 min.

The cylinder setup did not retrieve any pretreatment, except that it went through the same cleaning procedure as the cross section setup.

Tungsten

The circular cross-section of the tungsten wire was used as the active WE surface, similar to the setup for the glassy carbon electrode in Figure 4.4.1b. The wire was protected by a Teflon tube, and the wire end was cast into epoxy. This was done to cover the transition between the Teflon

tube and the wire. The electrode was then abraded with 350, 550, 850, 1000 and 2000 Si grit paper until the surface was shiny and even. Before an experiment, it was cleaned with distilled water, ethanol and acetone and air dried.

Platinum

Platinum sheets were cut into $1\,\mathrm{cm}^2 \times 1\,\mathrm{cm}^2$ pieces which served as the active WE area. The metal squares were further melted together with threads of their respective metal (see Figure 4.5.1). Teflon tubes were shrunk on the metal threads to isolate the exposed electrode area. Ideally, one side of the metal plate should be coated to control the current flow. However, due to the high value, and few samples, the metal did not retrieve any pretreatment. Both sides of the metal plate were therefore active areas. The same washing procedure was also completed pre-experiment for the platinum electrodes.

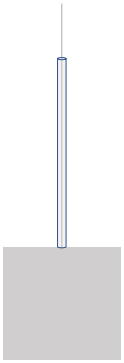

Figure 4.5.1: Design of the platinum electrode.

Copper

Copper electrodes were cut in L shape where the body was $1\,\mathrm{cm}^2 \times 2\,\mathrm{cm}^2$, and the exposed electrode area was $1.2\,\mathrm{cm}^2 \times 0.5\,\mathrm{cm}^2$. The electrode body was coated with several layers of Micro super XP2000 lacquer coating to isolate the active area (see Figure 4.5.2). To prepare the copper electrodes for coating, they were first cleaned with distilled water, ethanol, acetone and then air dried. Further, the active electrode area was covered with masking tape, and the electrode body was coated. Three layers were applied, and the coating was allowed to dry for one day after each layer was applied. Before the experiment, the masking tape was taken off, and the exposed electrode area was carefully cleaned with acetone and a Q-tip so that the coating did not detach from the electrode due to acetone's dissolution property.

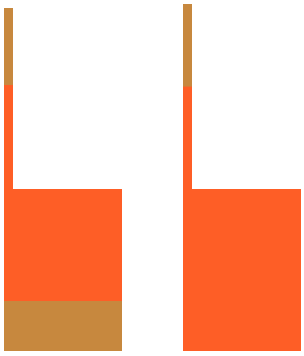

Figure 4.5.2: Design of copper electrode. The orange part represents the coating.

Aluminium

Aluminium was used as a working, reference and counter electrode. Two types of aluminium qualities were used, 1080 alloy sheets and 99.9998 % aluminium rod. The 1080 alloy was used as WE, CE and RE. When used as WE and CE, the sheets were cut into an L shape as the copper electrodes. For usage as a working electrode, the metal body was wrapped in Teflon tape to make a confined active area of 1 cm^2. As with platinum electrodes, aluminium electrodes were active on both sides of the metal. When used as a reference electrode, the alloy was cut into a thin bar. The 99.9998 % aluminium rod was used for reference and counter electrode and was used as it was. Before the experiments, the aluminium electrodes were left in 32 % HCl for 10 seconds to remove excessive oxide layers and then cleaned with distilled water and acetone.

4.6 Electrochemical measurements

The electrochemical measurements were carried out with a three-electrode setup, in the fume hood. Before experiments, the electrochemical cell was assembled in the glove box and then transferred out. The potentiostat used was Metrohm Autolab PGSTAT 302N with the control software NOVA.

4.6.1 Electrochemical impedance spectroscopy

Electrochemical impedance spectroscopy was performed before cyclic voltammetry experiments to find the electrolyte resistance. The data was used to IR compensate during cyclic voltammetry (in-situ IR compensation) and correct the remaining IR drop during data processing (post IR correction). The settings used for EIS are presented in Table 4.6.1. The measurements were performed at open circuit potential (OCP). The settings were slightly different for experiments in the cell with and without a separated reference electrode. As the potentiostat could not register the impedance at high frequency when the reference electrode was separated with a glass frit.

Table 4.6.1: Settings for electrochemical impedance spectroscopy. The measurements were done against OCP.

Cell	Amplitude	Start frequency	End frequency
Separated RE	5 mV	30 kHz	100 Hz
Not separated RE	5 mV	300 kHz	100 Hz

4.6.2 Cyclic voltammetry

Cyclic voltammetry was performed to establish an overview of the $AlCl_3$-urea system under different conditions, e.g., temperature variations and variation of the electrolyte composition. The experimental parameters are shown in table 4.6.2. All experiments started at OCP, and the potential was first swept in cathodic direction with the exception of experiments where the anodic reactions were studied. In these experiments, the potential was first swept in the anodic direction. Due to the high resistance in the electrolyte, 80 % of the resistance found from electrochemical impedance measurement was in-situ compensated during cyclic voltammetry measurements. The remaining resistance was post IR corrected to acquire voltametric data that would be close to the electrochemical behaviour without IR-drop.

Table 4.6.2: Experimental parameters for cyclic voltammetry

Working electrode	Electrolyte $AlCl_3$:urea:NaCl	Sweep rate [V/s]	Upper limit [V]	Lower limit [V]	Start dir. -
GC (0.2 cm^2)	1.5:1	0.1	1.3	- 0.3	cathodic
GC (0.2, 0.8 cm^2)	all electrolytes	0.1	1.3	-0.5	cathodic
GC (0.2 cm^2)	all electrolytes	0.1	1.3	-1.5	cathodic
GC (0.8 cm^2)	1.5	0.1	1.5	-1.5	cathodic
GC (0.03 cm^2)	1.3:1, 1.5:1	1	1.3	-1.5	cathodic
1080 Alloy , Pt, W	1.5:1	1	8	-0.3	cathodic
Graphite (0.94 cm^2)	1.5:1	0.1	2.5	-0.3	cathodic
Pt, W, Graphite (0.3 cm^2), GC (0.2 cm^2)	1.5:1, 1.5:1:0.35	0.1	3	0.3	anodic
GC (0.2 cm^2)	1.5:1	0.1	2	0.3	anodic

Temperature variation experiment

Cyclic voltammetry measurements as a function of temperature were done in a silicon oil bath. The oil was heated with a combined hot plate and magnetic stirrer. A magnet was left in the oil bath, and one was left in the electrolyte to distribute the heat quicker.

4.6.3 Chronoamperometry

Chronoamperometry was used for in-depth investigation of some of the possible electrochemical reactions.

4.6.4 Cleaning

After the experiments, the electrodes were cleaned with acetone and distilled water and left to dry.

4.7 Scanning electron microscopy

SEM pictures were taken after chronoamperometry experiments, and the instrument settings for detecting SE are given in 4.7.1. The magnification varied depending on the investigated electrode material. An EDS analysis was performed after aluminium deposition to identify the deposit composition.

Table 4.7.1: Instrument settings for SE detection.

Setting	Value
Mode	SE
Electron volt	10 kV
Probe current	40.0

Chapter 5

Results

5.1 Preparation of the electrolytes

The electrolyte compositions with and without NaCl given in table 4.2.1 were prepared according to the experimental procedure.

Some observations were made during the preparations of the electrolytes. During the mixing of the chemicals, the electrolyte was very sensitive, especially when making electrolytes with a high concentration of urea. If the temperature was above 40 °C, the electrode decomposed. Electrolytes with higher concentrations of $AlCl_3$ (e.g 1.5:1) was less temperature sensitive and could reach 70 °C without decomposing. Adding $AlCl_3$ to the mixture was an endothermic process which decreased the temperature while adding urea increased the temperature. Including NaCl, electrolyte became thicker (the viscosity increased). At 1.5:1:0.5 $AlCl_3$-urea-NaCl, the electrolyte was saturated with NaCl because additional NaCl did not dissolve into the melt, which is in accordance with Mamantov et al. [31].

To study the behaviour of $AlCl_3$-urea ILA in a humid atmosphere, 1:1, 1.3:1, and 1.5:1 $AlCl_3$-urea electrolytes were exposed to the atmosphere for 1 min and then left in the fume hood in closed vial glasses (Figure 5.1.1). The changes in the electrolyte over time was recorded. After eight days, the most notable changes were seen in the 1:1 electrolyte. With increased mole fraction of $AlCl_3$, the electrolyte seemed less reactive towards a humid atmosphere.

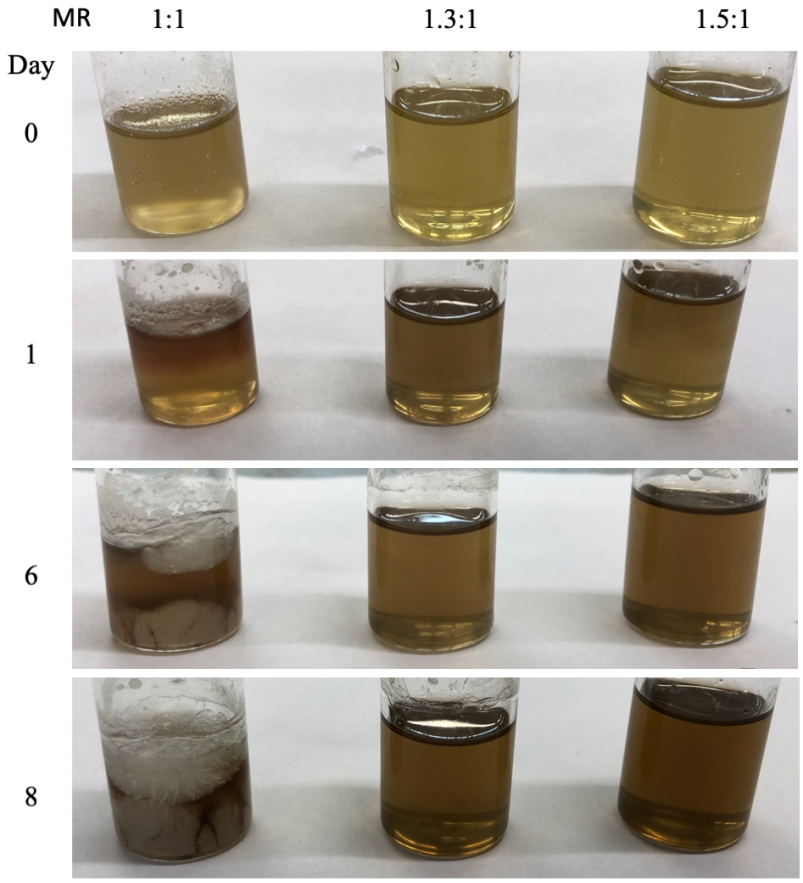

Figure 5.1.1: The development of the electrolyte over 8 days when stored in the fume hood (Figure 4.4.1a).

5.2 Raman spectroscopy

Raman spectroscopy was performed to identify the speciation in the electrolytes. Figure 5.2.1 shows the whole Raman spectrum (100 cm^{-1} to 3820 cm^{-1}) of the 1.5:1 $AlCl_3$-urea electrolyte. The peaks and their suggested compounds are given in Table 5.2.1. The peaks have been assigned based on the work of Frost et al. and Ferraro et al. for urea [52, 53], and Takahashi et al., Angell et al., and Gilbert et. al for the chloroaluminate anions [54, 12, 55]. Only the functional groups of urea were detected, and it was therefore hard to draw any conclusion about its speciation in the electrolyte.

Two observations of the spectrum are worth mentioning. The peak for molecular aluminium chloride at 340 cm^{-1} is not seen. OH-stretching peaks, on the other hand, are observed. The electrolyte should not have OH bondings, which indicates that the peaks are related to humidity impurities.

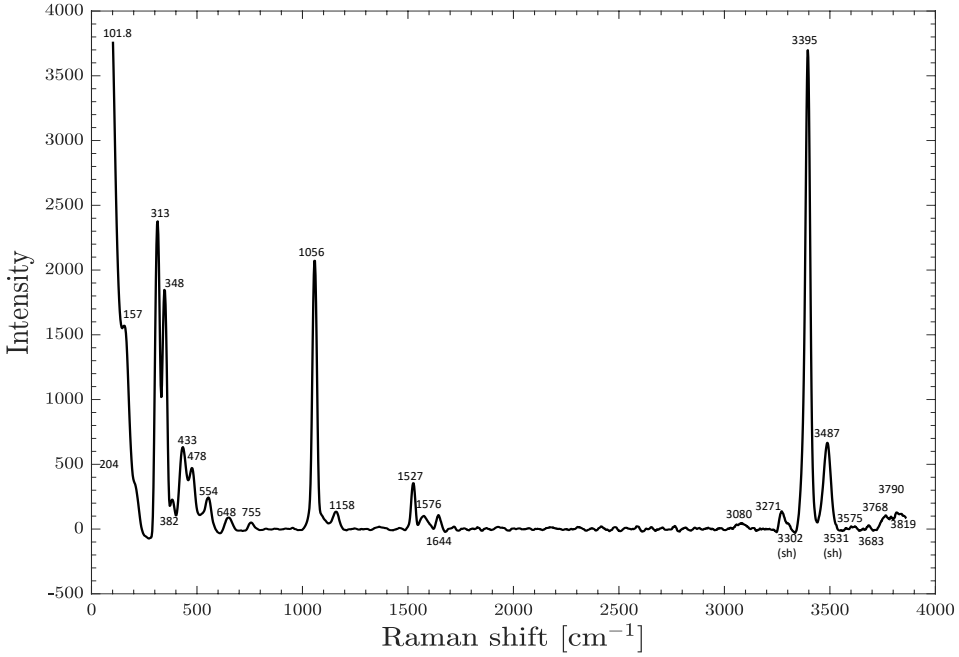

Figure 5.2.1: Raman spectra of the 1.5:1 electrolyte including the whole system.

Table 5.2.1: Raman shifts and their proposed compounds. The peaks designated for urea is based on the work of Frost et al. [52] and Ferraro et al. [53]. The proposed peaks for chloroaluminate species is based on the work of Takahashi et al., Angell et at. and Gilbert et al. [54, 12, 18].

Raman shift [cm^{-1}]	Compound
313	$Al_2Cl_7^-$
351	$AlCl_4^-$
383	$Al_2Cl_7^-$
433	$Al_2Cl_7^-$
476	-
554	NCN bend
650	-
757	-
1058	NCN stretch or rocking NH_2
1161	-
1526	-
1575	CO - H bond stretch
1645	CO - stretch
3272	NH -stretch
3300	NH -stretch
3395	NH -stretch
3489	NH -stretch
3556	-
3575	-
3578	-
3602	OH stretching
3620	OH stretching
3659	-
3685	OH stretching
3764	-
3790	-
3817	-

The Raman spectra of the electrolytes were then compared in the range 200 cm^{-1} to 700 cm^{-1} to study the relationship between $Al_2Cl_7^-$ and $AlCl_4^-$. Figure 5.2.2 shows the Raman spectra of $AlCl_3$-urea and $AlCl_3$-urea-NaCl melts with different compositions between 1:1:0 and 1.5:1:0.5. The Raman spectra are normalized to the $AlCl_4^-$ peak at 351 cm^{-1} and the legends are sorted after increasing intensity of the $Al_2Cl_7^-$ peak at 313 cm^{-1}.

From the figure, it is seen that the peak intensity of $Al_2Cl_7^-$ depends on the mole fraction of $AlCl_3$. At a 1:1 mixture, the $Al_2Cl_7^-$ peak is absent. By adding $AlCl_3$ to a mole ratio of 1.3:1, a small peak is seen, and at a mole ratio of 1.5:1, the peak intensity of $Al_2Cl_7^-$ is larger than the peak of $AlCl_4^-$. The opposite is occurring when the mole fraction of NaCl is increasing; the peak intensity of $Al_2Cl_7^-$ decreases. At 1.5:1:0.5 mole ratio, the $Al_2Cl_7^-$ peak is negligible, and the associated spectrum is quite similar to the spectrum of the 1:1 electrolyte.

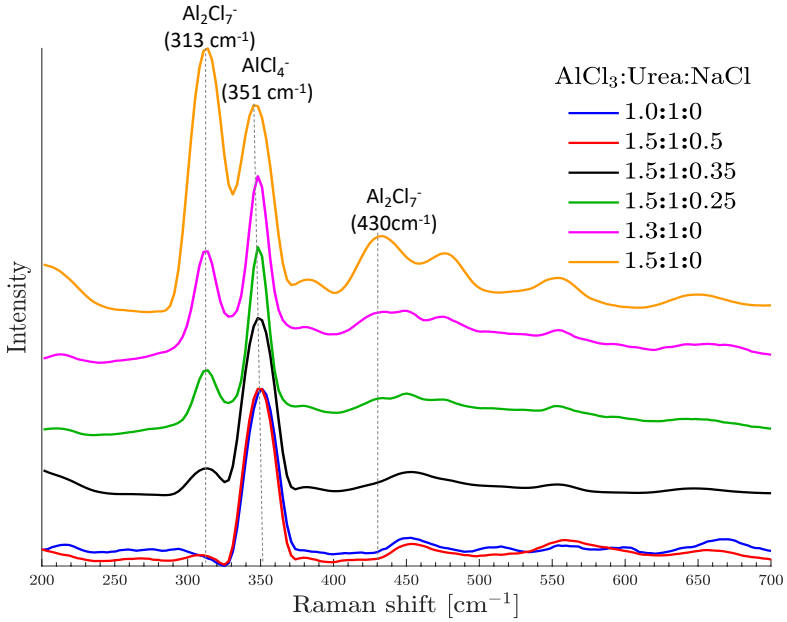

Figure 5.2.2: Electrolyte speciation study of electrolytes with and without NaCl The spectra are plotted in the order of increasing $Al_2Cl_7^-$ (313 cm^{-1}) peak. The spectra are normalized to the $AlCl_4^-$ (315 cm^{-1}) peak.

The relative concentrations of the ionic complexes in the melt were estimated to get a brief understanding of the electrolyte composition. To calculate the relative concentration, equation 2.2.3 was used and the results are shown in Table 5.2.2. The concentration of $[Al_2Cl_7^-]/[AlCl_4^-]$ and $[[AlCl_2(urea)_2]^+]/[Al_2Cl_7^-]$ in the 1.3:1 electrolyte was found to be 0.66 and 2.51, respectively, and the values are therefore close to 0.6 and 2.6 reported by Angell et al. [12].

Table 5.2.2: Relative concentration of the ionic species in the $AlCl_3$-urea electrolyte. The values given in parenthesis is reported by Angell et al. [12].

Mole ratio ($AlCl_3$:urea)	$[Al_2Cl_7^-]/[AlCl_4^-]$	$[AlCl_2(urea)_2^+]/[Al_2Cl_7^-]$
1:1:0	-	-
1.3:1:0	0.66 (0.6)	2.51 (2.6)
1.5:1:0	1.51	1.66

5.3 The effect of IR-drop and IR-compensation

Compared to many other electrolytes, the $AlCl_3$-urea electrolyte has low ionic conductivity. The measurement must, therefore, be compensated for the associated IR-drop. The electrolyte resistance was measured by using EIS, and different procedures of compensation were tested. The experiment was performed in a 1.5:1 electrolyte on a glassy carbon working electrode with a 0.2 cm^2 large area and the sweep rate was 0.1 V/s.

Figure 5.3.1a shows the result of an uncompensated voltammogram compared with the effect of a 50 % in-situ compensation, a 50/50 % in-situ compensation and post-IR correction and 100 % post IR-correction at 25 °C. From the figure, it is seen that the IR-corrected voltammograms (b and d) overlap each other, but the current density at the cathodic turning point for voltammogram b is lower than d, indicating that the post-IR-correction performs worse on less in-situ IR compensated voltammograms.

In Figure 5.3.1b, a fully in-situ IR compensated voltammogram is compared with voltammograms at 85 % and 80 % in-situ compensation. It is seen sharp current peaks at both 100 % and 85 %, but the peak is less intensive for the latter. Current peaks like these are atypical for metal deposition and stripping, and most likely the voltammograms are overcompensated. At 80 % in-situ compensation, the sharp peaks are not seen, and the compensation degree is therefore stable. The voltammogram is however stretched out compared to a voltammogram of metal deposition/stripping without IR-drop, and the remaining uncompensated IR-drop needs to be post-IR-corrected.

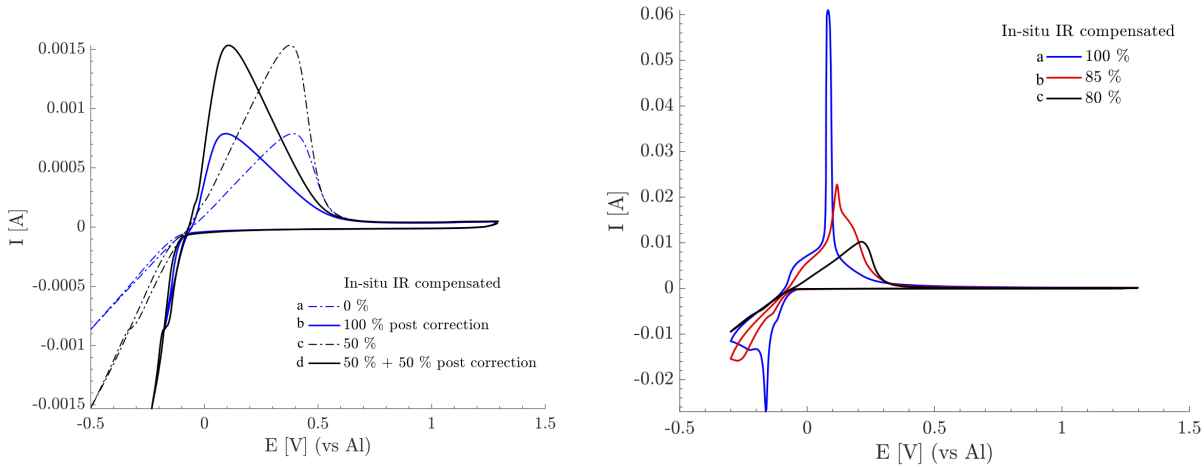

Figure 5.3.1: The effect of IR-compensation on the voltammogram. The voltammograms were recorded in a 1.5:1 electrolyte at a sweep rate of 0.1 V/s. The working electrode was a glassy carbon rod with an active area of 0.2 cm^2. (a) A comparison of different degrees of post IR-correction and in-situ IR compensation. T = 25 °C. (b) A comparison of in situ compensation at 100 %, 85 % and 80 %. T = 75 °C.

5.4 Working electrode material

Working electrodes of glassy carbon and tungsten were used to study the aluminium deposition process. Cyclic voltammograms on these materials were compared to investigate the effect of different substrates on the deposition and stripping reactions. The results were compared to an experiment where Al was used as a working electrode. The voltammograms were recorded in a 1.5:1 electrolyte with a sweep rate of $0.1\,\mathrm{V/s}$, and they are shown in Figure 5.4.1. It is seen that aluminium deposition on glassy carbon and tungsten is quite similar; they both require a nucleation overpotential. Aluminium deposition, on the other hand, occurs without a nucleation overpotential, and the current density becomes slightly higher in the potential window.

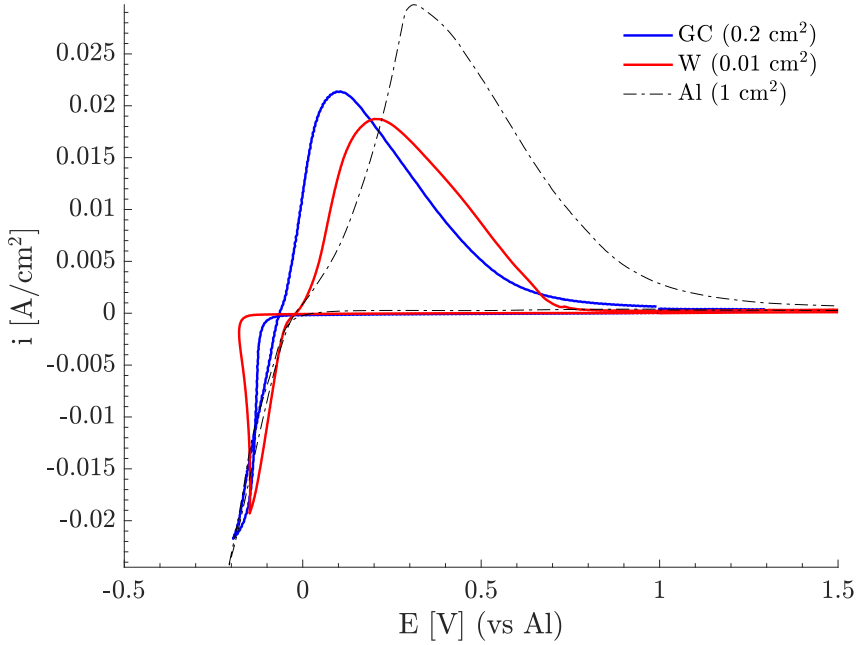

Figure 5.4.1: Deposition and stripping on GC and W working electrode compared with an Al working electrode

5.5 Cathode processes

The different compositions of $AlCl_3$-urea and $AlCl_3$-urea-NaCl electrolyte were investigated with cyclic voltammetry. The sweep rate used was $0.1\,V/s$ and the working electrode was glassy carbon with an active area of $0.2\,cm^2$ for all measurements, except for measurements in the 1.3:1 and 1.5:1 electrolyte. For these two electrolytes, the sweep rate was $1\,V/s$, and the working electrode was $0.03\,cm^2$. The separate procedure for 1.3:1 and 1.5:1 electrolyte was chosen due to technical problems with the potentiostat. The potentiostat could not in-situ compensate 80 % at the required current range, resulting in under compensated voltammograms. The active electrode area was therefore reduced, and the sweep rate was chosen to limit the amount of aluminium deposition because the aluminium tended to glide off the electrode, causing noise to the voltammogram.

Figure 5.5.1 shows the resulting voltammograms. The legends are sorted after increasing $[Al_2Cl_7^-]/[AlCl_4^-]$ concentration. In the set potential window, no current response is seen from the 1:1 and the 1.5:1:0.5 electrolyte, whereas a rising cathodic current density, is seen in the other electrolytes close to the reference potential (0 V). During the specialization project, the rising current density was ascribed to aluminium deposition [56]. It is seen that the onset potential for aluminium deposition depends on the $Al_2Cl_7^-$ concentration. With decreasing $Al_2Cl_7^-$ concentration in the melt, the onset potential is shifted to higher cathodic potentials. At a given potential, The cathodic current density also decreases with decreasing $Al_2Cl_7^-$ concentration.

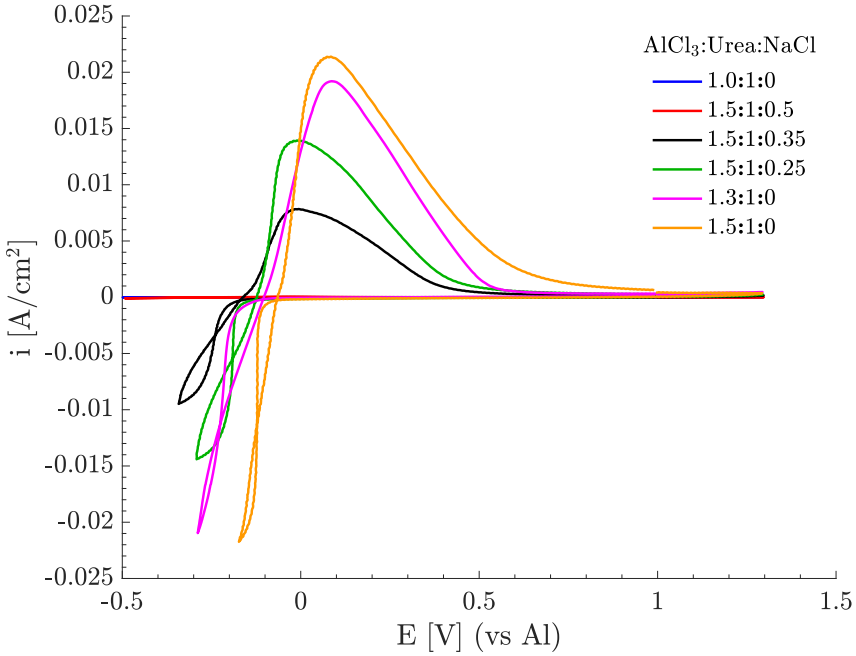

Figure 5.5.1: Cyclic voltammogram study of the electrolytes. The sweep rate was 0.1 V/s and the working electrode was GC with an area of 0.2 cm^2 for all electrolytes except the 1.3:1 and 1.5:1 electrolyte. Due to technical reasons, they were recorded on 0.03 cm^2 GC and with a sweep rate of 1 V/s. The legend is organized after increased relative mole ratio of $Al_2Cl_7^-$:$AlCl_4^-$.

Figure 5.5.2a and 5.5.2b shows cyclic voltammograms recorded in the same electrolytes as above, where the electrochemical window has been expanded. In Figure 5.5.2b, the voltammograms of 1.5:1 and 1.3:1 electrolyte has been left out. Unlike the other electrolytes, the current

density related to aluminium deposition from the 1.3:1 and 1.5:1 electrolyte does not seem to reach a peak current density. The rate of aluminium deposition from 1.3:1 electrolyte, does, however, seem to reach a plateau. The stripping reaction in these two electrolytes is stretched out and seem to continue until around 1.7 V.

For the other electrolyte compositions, another reaction is seen at higher cathodic potentials (Figure 5.5.2b). It starts at around $-0.9\,\mathrm{V}$ for the 1.5:1:0.25 electrolyte and shifts to even higher cathodic potentials with decreasing $Al_2Cl_7^-$ concentration in the melt. There are no corresponding oxidation current densities immediate to the reduction potential. The onset stripping potential for the 1.5:1:0.25 and 1.5:1:0.35 had however shifted roughly 200 mV compared to the stripping reaction in the same electrolytes when the electrochemical window was $-0.5\,\mathrm{V}$ to $1.3\,\mathrm{V}$. The 1:1 and 1.5:1:0.5 electrolytes, which did not show any current response in the electrochemical window of $-0.5\,\mathrm{V}$ to $1.3\,\mathrm{V}$ have an oxidation peak starting close to the stripping potential of aluminium, indicating that the oxidation reaction might be related to the reaction at about -1.1 V, but has been shifted to more positive potentials.

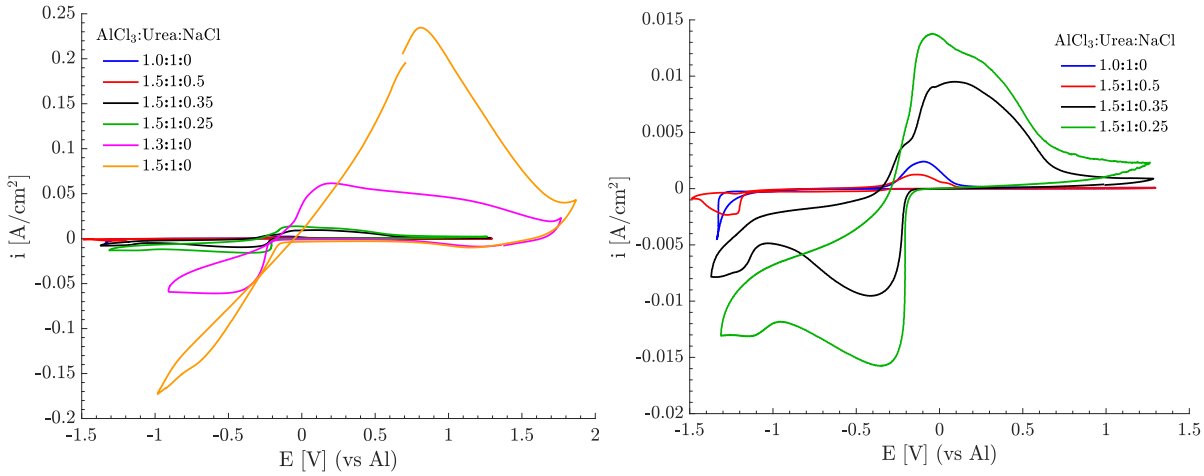

Figure 5.5.2: Cyclic voltammogram study of the electrolytes. The sweep rate was 0.1 V/s and the working electrode was GC with an area of 0.2 cm^2 for all electrolytes except the 1.3:1 and 1.5:1 electrolyte. Due to technical reasons, they were recorded on 0.03 cm^2 GC and with a sweep rate of 1 V/s. The legend is organized after increased relative mole ratio of $Al_2Cl_7^-$:$AlCl_4^-$.(a) All electrolytes (b) Without 1.3:1 and 1.5:1 electrolytes.

5.5.1 Chronoamperometry of a 1.5:1:0.5 $AlCl_3$-urea-NaCl

Chronoamperometry was performed in a 1.5:1:0.5 $AlCl_3$-urea-NaCl electrolyte to confirm the nature of the electrochemical process occurring at around $-1.1\,\mathrm{V}$. The electrolyte was chosen instead of the 1:1 $AlCl_3$-urea electrolyte because NaCl acts as a buffer and the electrolyte will be closer to a neutral melt than a prepared 1:1 $AlCl_3$-urea. Also, from Figure 5.5.2b, the onset potential for the reaction around $-1.1\,\mathrm{V}$ did not seem to be largely affected by the addition of NaCl.

A cyclic voltammogram was recorded before electrolysis to determine the potential of the reaction at higher cathodic potentials (Figure 5.5.3a). This was done because the reference potential

(0 V) would shift in the electrolysis cell due to a different setup of the pseudo-reference electrode (Figure 4.4.1a). The cathode and working electrode in the electrolysis and the cyclic voltammetry was 0.5 cm^2 and the electrolysis potential was set to -1 V (vs Al). It is observed that the deposition reaction occurs at a lower cathodic potential compared to using the electrode cell in Figure 4.4.1b. The potential difference between the reduction and oxidation reaction is, however, the same and it is therefore assumed to be the same reaction. Figure 5.5.4a, and 5.5.4b, shows the copper electrode after 500 s electrolysis in the electrolyte after it has been cleaned with acetone. It was observed bubbles on the cathode in addition to a dark grey deposit, meaning that gas evolution also occurs at this potential. The deposit did not adhere well to the electrode after it was taken out of the electrolyte and most of it fell off when the electrode was cleaned with acetone. EDS analysis however, showed aluminium oxide particles on the electrode, indicating that the dark grey deposit was aluminium.

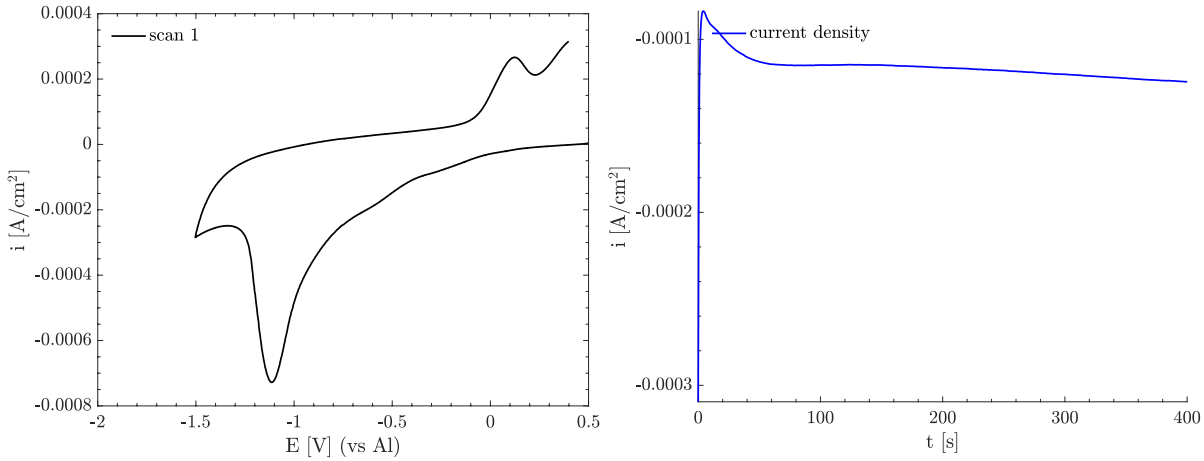

(a) **(b)**

Figure 5.5.3: (Electrochemical measurements in the 1.5:1:0.5 electrolyte a) Cyclic voltammetry. The working electrode was copper with an active area of 0.5 cm^2 and the sweep rate was 0.1 V/s (b) Chronoamperometry at -1 V for 400 s.

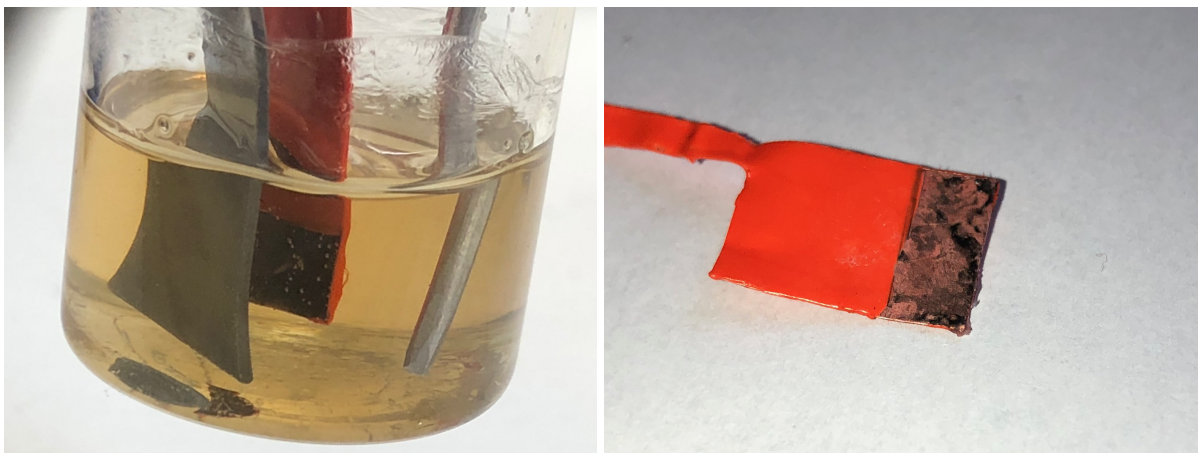

(a) **(b)**

Figure 5.5.4: Pictures of the working electrode. (a) In the electrolyte during chrono amperometry. (b) After it was cleaned.

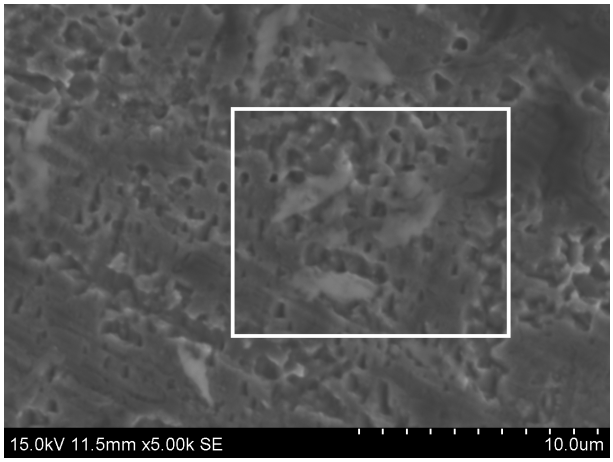

(a)

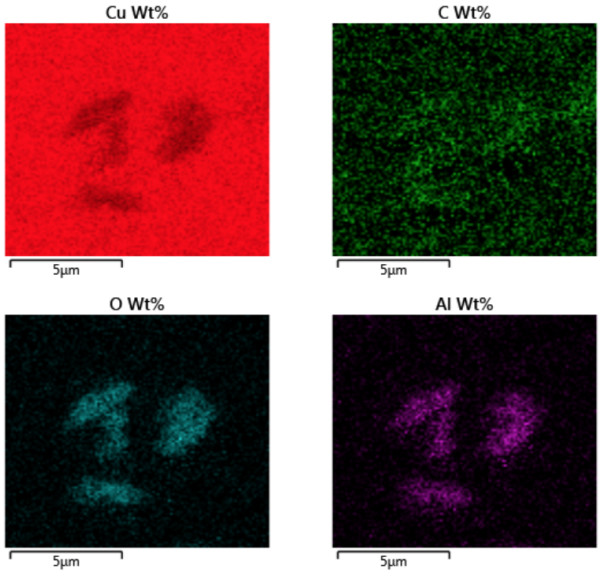

(b)

Figure 5.5.5: SEM picture and EDS analysis of the working electrode. (a) SEM picture. The white frame indicates the EDS analysis area. (b) EDS analysis.

5.5.2 The effect of sweep rate

Cyclic voltammograms for the 1.3:1 and 1.5:1 electrolyte as function of sweep rate are shown in Figure 5.5.6a and 5.5.6b, respectively. At 0.01 $\mathrm{V/s}$ it is observed that the current density on the cathodic sweep is reaching a limiting current at about $-0.15\,\mathrm{V}$ for 1.5:1 V and $-0.18\,\mathrm{V}$ for 1.3:1 electrolyte. The behaviour is seen more clearly in the 1.3:1 electrolyte as the current density is reaching an obvious plateau. Studying the stripping peaks, they do not seem to vary a lot with the increase of sweep rate, indicating that the sweep rate does not affect the voltammogram a lot.

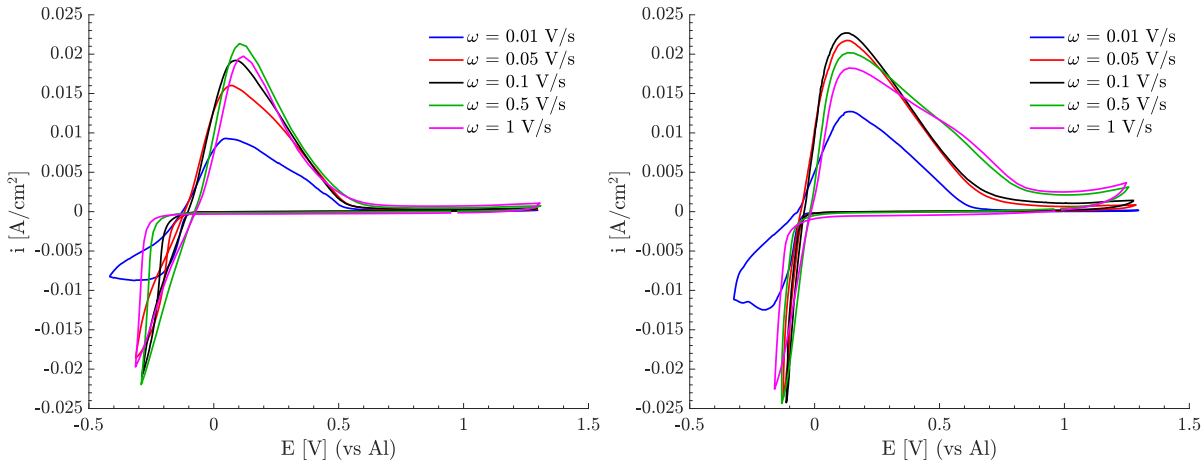

(a) 1.3:1 **(b)** 1.5:1

Figure 5.5.6: 1.3:1 and 1.5:1 $AlCl_3$-urea as function of sweep rate on 0.2 cm^2 GC

5.5.3 The effect of temperature

The effect of temperature on the aluminium deposition/stripping reaction and ion conductivity in a 1.5:1 $AlCl_3$:urea melt was studied. Figure 5.5.7 shows cyclic voltammograms recorded at different temperatures on glassy carbon with an area of 0.2 cm^2. The sweep rate was 0.1 V/s. The electrolyte resistances were found by using EIS, and the resistance as a function of temperature is presented in Figure 5.5.8a. An Arrhenius plot of the specific conductivity was derived from the recorded resistances, and the figure is shown in 5.5.8b. The plot seems to follow an Arrhenius behaviour, and the activation energy for the specific conductivity was found to be 0.25 eV. The error for the activation energy is not calculated as it depended on too many factors.

It is seen that the resistance decreases, and thus, the conductivity increases with temperature. The increased temperature reflects in the cyclic voltammograms, and the cathodic turning current density also depends on the temperature. The characteristic crossover found in metal deposition/stripping voltammograms is gradually disappearing with increasing temperature and at 75 °C the current for the forward and reverse sweep does not cross each other.

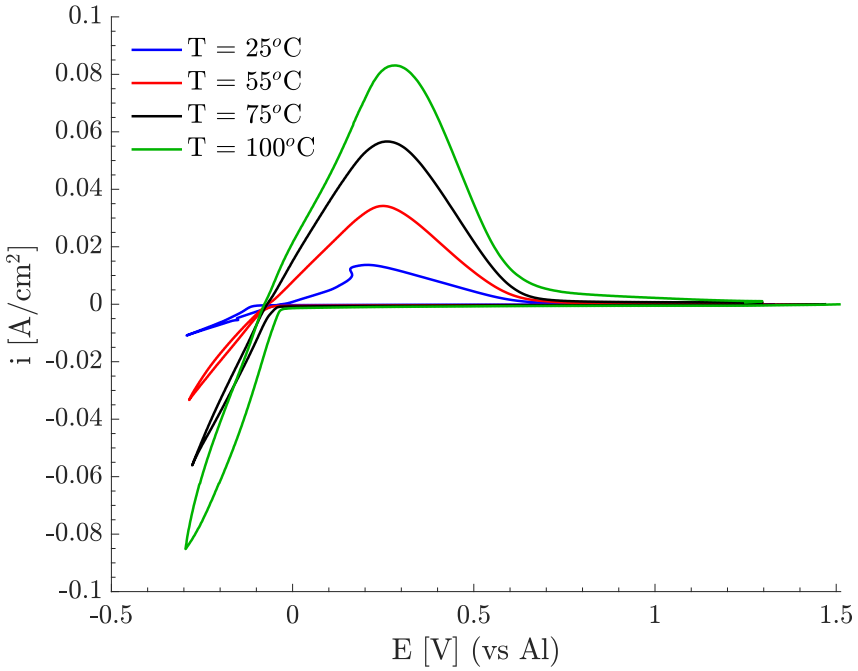

Figure 5.5.7: Cyclic voltammograms recorded in a 1.5:1 electrolyte at different temperatures with a sweep rate of 0.1 V. The working electrode was glassy carbon with an area of 0.8 cm^2.

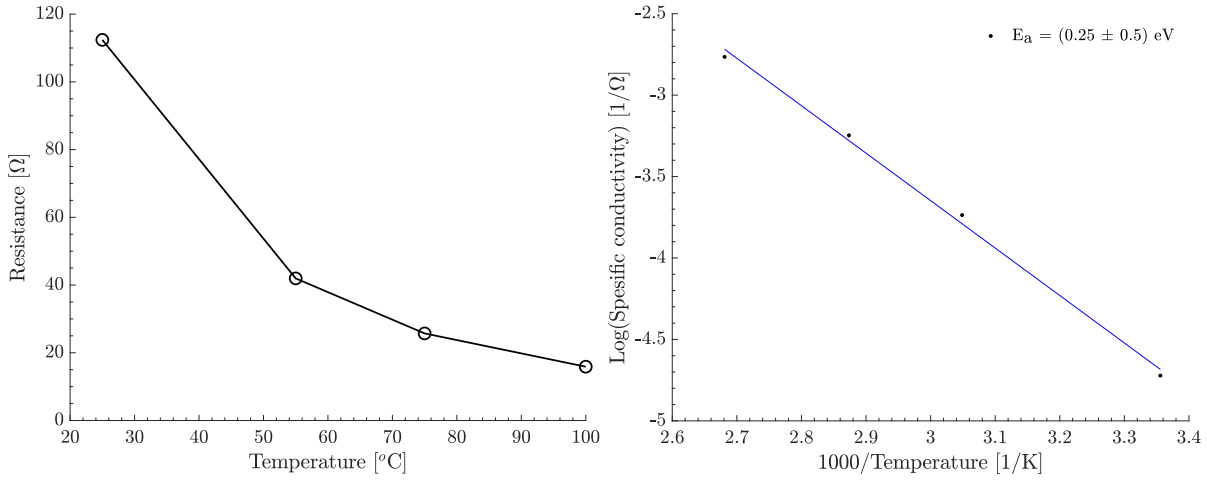

(a) **(b)**

Figure 5.5.8: Resistance and specific conductivity in the 1.5:1 electrolyte. (a) Electrolyte resistance plotted as function of temperature. (b)Arrhenius plot of the specific conductivity.

A cyclic voltammogram with a potential window of $-1\,\mathrm{V}$ to $1.3\,\mathrm{V}$ was recorded at $100\,^{\circ}\mathrm{C}$ to investigate the reaction at higher cathodic potentials. Figure 5.5.9a shows the cyclic voltammetry recorded on a $0.2\,\mathrm{cm}^2$ GC and with a sweep rate of $0.1\,\mathrm{V/s}$. It is observed that the aluminium deposition reaction, reaches some current density limits around $-0.4\,\mathrm{V}$ as it reaches a plateau. The current density, however, starts to increase right after at around $-0.6\,\mathrm{V}$, which could be related to the second process at a higher cathodic potential. During the cyclic voltammetry, it was observed that the deposited aluminium did not adhere to the electrode, but glided off as a thick dark cloud, as shown in Figure 5.5.9b. Due to this, the consecutive sweeps jumped wildly and did not give any meaningful data. An example is shown in the Appendix, Figure A.0.1

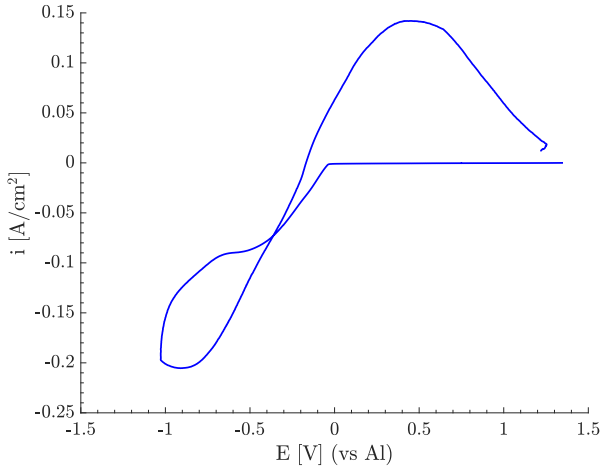

(a)

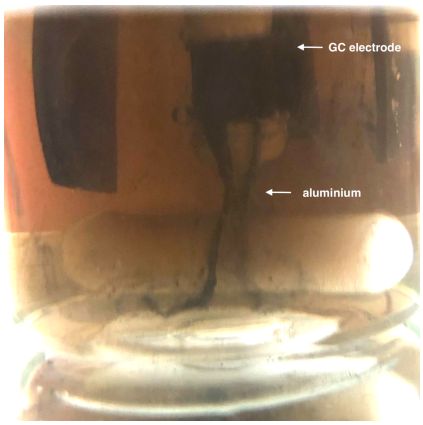

(b)

Figure 5.5.9: Cyclic voltammogram in a 1.5:1 electrolyte with a scan rate of $0.1\,\mathrm{V/s}$ at $100\,^{\circ}\mathrm{C}$. The working electrode was glassy carbon with an active area of $0.8\,\mathrm{cm}^2$ (a) The voltammogram (b) Picture of the aluminium gliding of the electrode during cyclic voltammetry.

5.6 Anode processes

Several anode processes have been observed in the $AlCl_3$-urea melt depending on the electrode material and if the electrolyte contains NaCl. Due to that, the results have been presented according to the electrolyte type. First, the anode processes occurring in $AlCl_3$-urea melts will be presented, then the anode processes in $AlCl_3$-urea-NaCl melts. The cyclic voltammetry measurements started with anodic polarization if it is not mentioned otherwise.

5.6.1 The $AlCl_3$-urea electrolyte

The 1.5:1 electrolyte was chosen for studies on the anode processes in melts without NaCl because the melt has shown to be the most promising for aluminium deposition, i.e. high cathodic current density for the observed electrochemical windows. If not indicated otherwise, the set sweep rate for cyclic voltammetry was $0.1\,\mathrm{V/s}$

The anodic limit of the electrolyte was first investigated. Cyclic voltammetry measurements were performed on an aluminium electrode with an area of $1\,\mathrm{cm}^2$. The electrochemical window was between $-0.1\,\mathrm{V}$ to $8\,\mathrm{V}$. Figure 5.6.1a shows the voltammogram and Figure 5.6.1b shows a snippet of the voltammogram between 2 V and 8 V. It is seen that the stripping current is slightly higher than the deposition current. This could indicate that the dissolution of aluminium is also occurring. The current density decreases to $0.6\,\mathrm{mA\,cm^{-2}}$ at around $2\,\mathrm{V}$ and it is seen to continue in this current range, never dropping below zero. Other than these current responses, there is not seen any other reactions in this potential range.

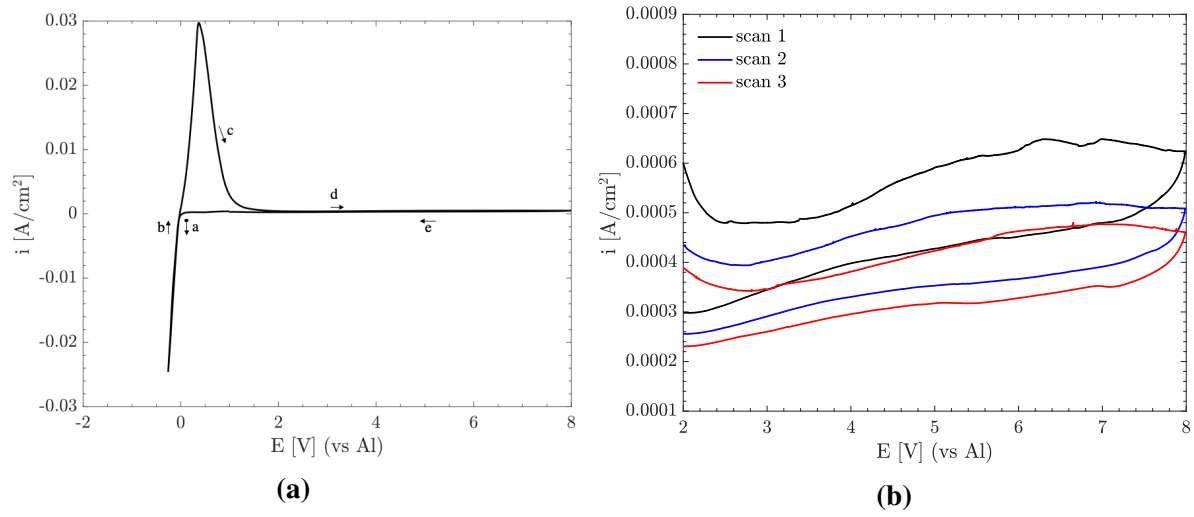

Figure 5.6.1: Cyclic voltammograms on a $1\,\mathrm{cm}^2$ Al electrode. (a) with aluminium deposition and stripping (b) A zoom on the aluminium dissolution.

It was then continued with a study of the anode processes on carbon materials. Figure 5.6.2a shows the voltammograms on a glassy carbon working electrode with an area of $0.2\,\mathrm{cm}^2$. As seen from the voltammogram, a rising anodic current density starts at around $1.5\,\mathrm{V}$. Consecutive scans showed that the voltammograms did not deviate much, indicating that the process was chemically reversible process (Figure A.0.2 in Appendix A). After the measurement, it was observed that the blank electrode surface had become rough, indicating an intercalation process.

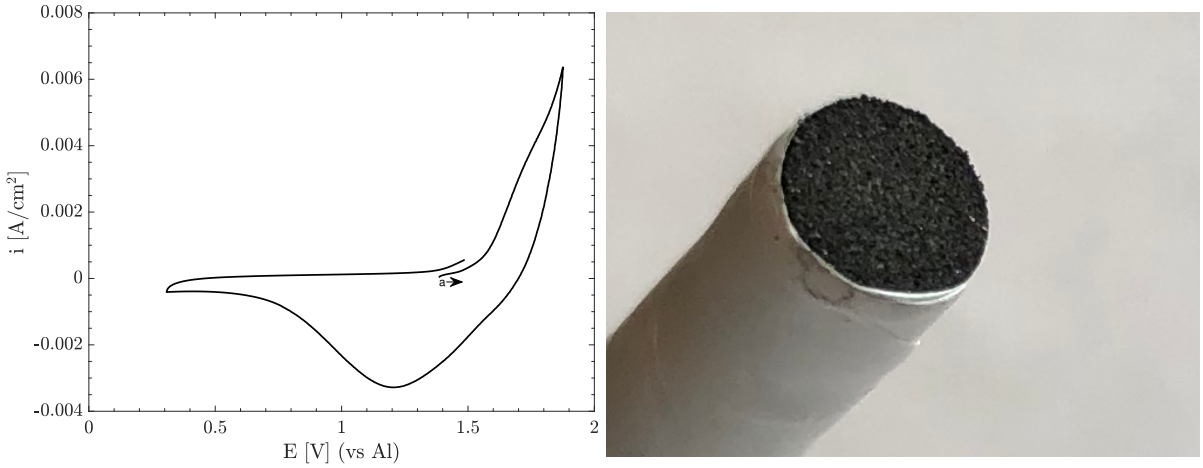

(a) **(b)**

Figure 5.6.2: Cyclic voltammetry on a $0.2\,\mathrm{cm}^2$ GC with a sweep rate of $0.1\,\mathrm{V/s}$ (a) The resulting voltammogram (b) Electrode surface after measurements.

Figures 5.6.3a and 5.6.3b show cyclic voltammograms on respective graphite with an area of $0.35\,\mathrm{cm}^2$ and glassy carbon with an area of $0.2\,\mathrm{cm}^2$, where the electrochemical window has been expanded in the anodic direction to 3 V. The voltammograms are not post IR corrected because the electrode disintegrated during the anodic polarization, resulting in strange current responses. It is seen that the voltammogram on glassy carbon reaches a plateau on the anodic sweep at around 2.3 V. This is artefacts, due to the limitation of the chosen current range.

There are some similarities between the voltammogram of graphite and glassy carbon. They follow the same path, and most likely, it is the same reaction. The voltammogram of glassy carbon would probably look the same as the graphite if it did not reach the current range limit. Two reactions are occurring in this potential window. The first reaction occurs at 1.5 V, which was seen on glassy carbon and a second reaction at around 2.4 V. It is believed that the second reaction leads to the disintegration of the electrode.

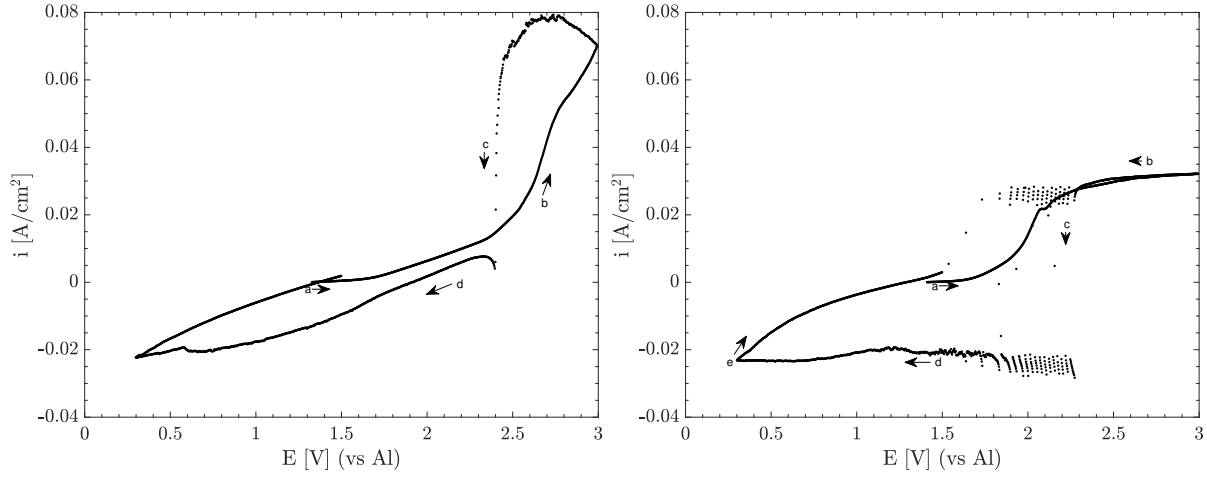

(a) **(b)**

Figure 5.6.3: Cyclic voltammogram on carbon electrodes with a sweep rate of $0.1\,\mathrm{V/s}$. (a) Graphite working electrode with an area of $0.35\,\mathrm{cm}^2$. (b) Glassy carbon working electrode with an area of $0.2\,\mathrm{cm}^2$

Figures 5.6.4a and 5.6.4b show the voltammograms on respectively tungsten ($0.01\,cm^2$) and platinum ($2\,cm^2$) with the same potential window. A reaction starts to occur around 2.5 V on tungsten and 2.3 V on platinum. The corresponding reduction reaction is shifted to more cathodic potentials, indicating that the reaction is to some degree, irreversible. There are some similarities between the voltammograms, and their difference in size and material might explain the differences.

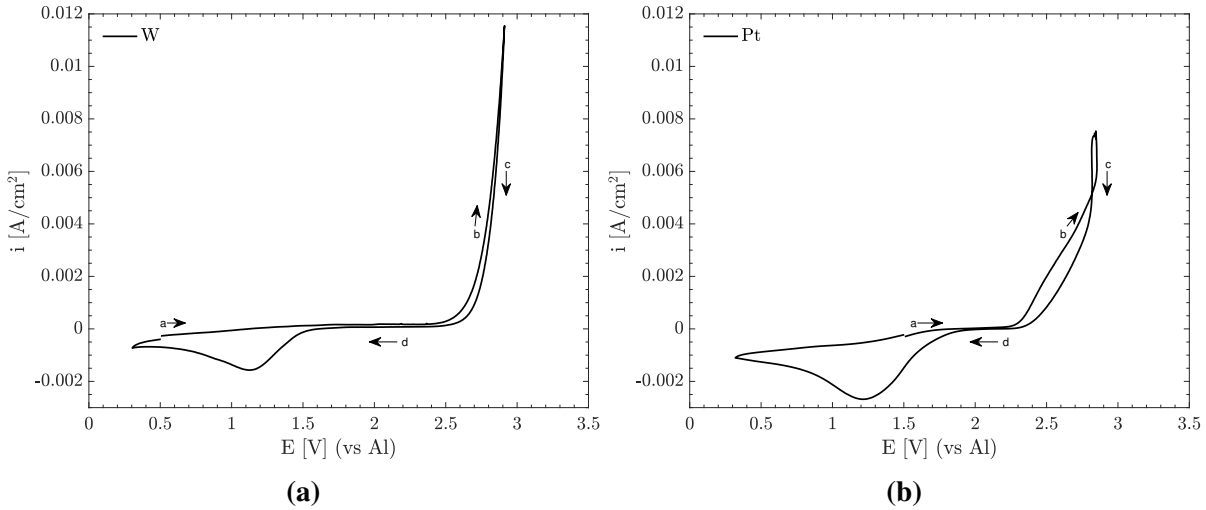

Figure 5.6.4: cyclic voltammograms recorded with a sweep rate of $0.1\,V/s$ in a 1.5:1. (a) W. (b) Pt.

Figures 5.6.5a and 5.6.5b show the voltammograms on W ($0.01\,cm^2$) and Pt ($2\,cm^2$) when the potential window is set to 8 V. It is seen that the reaction earlier reaches a peak the current density decrease to almost zero. There is, however, always current flowing, and it is larger on platinum. Most likely, the current is related to metal dissolution. There is no reduction peak associated with the oxidation peak like earlier.

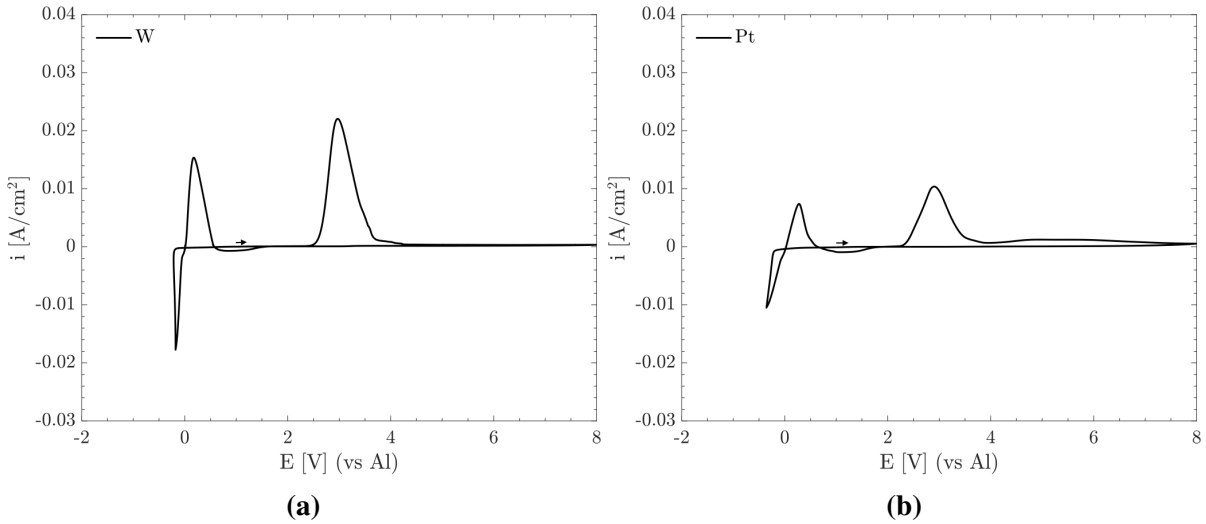

Figure 5.6.5: cyclic voltammograms recorded with a sweep rate of $0.1\,V/s$ in a 1.5:1. The measurement started in cathodic direction. (a) W. (b) Pt.

The reaction on platinum at around 2.3 V, was then investigated by chronoamperometry. Figure 5.6.6a shows the variation of current density with time and Figure 5.6.6b shows the electrode after the experiment. A yellow film formed on the platinum electrode over time. The current density did not reach steady state, but continued decreasing. This indicates that the film, to some extent, hinders further electrochemical processes. The film was sensitive to humid atmosphere and reacted quickly, with the same reaction behaviour as the electrolyte.

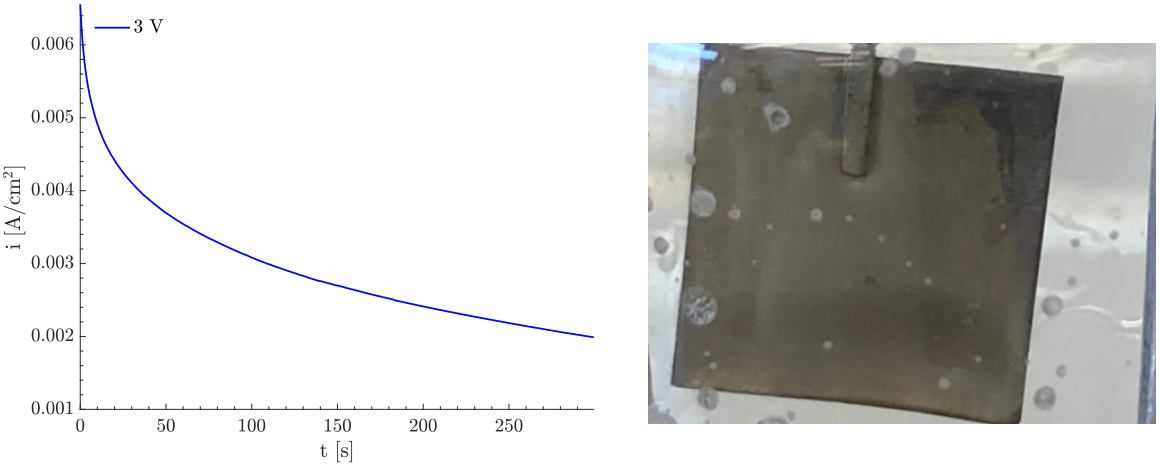

(a) **(b)**

Figure 5.6.6: Chrono amperometry on a 2 cm^2 platinum sheet at 3 V for 5 min and the resulting product. (a) Chrono amperometry (b) The product on Pt

5.6.2 $AlCl_3$-urea-NaCl electrolyte

The 1.3:1:0.35 electrolyte was chosen for the investigation of the $AlCl_3$-urea-NaCl electrolyte. The sweep rate for voltammetry measurements was $0.1\,V/s$

Figure 5.6.7 shows a cyclic voltammograms recorded on a $2\,cm^2$ platinum working electrode. A reaction starts at around 2.3 V, similar to reaction on Pt in $AlCl_3$-urea melts.

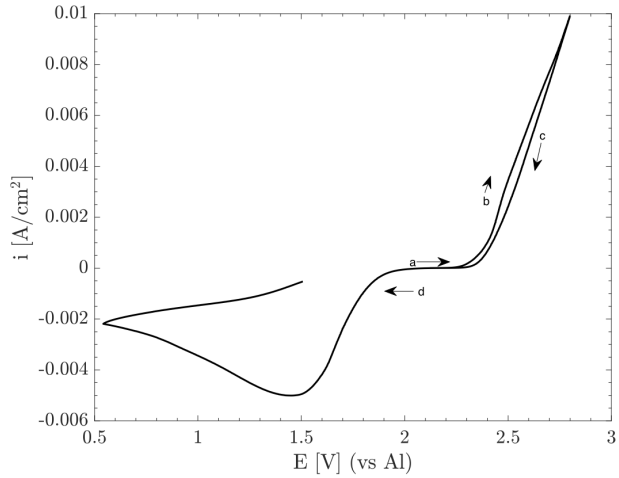

Figure 5.6.7: Cyclic voltammetry on a $2\,cm^2$ platinum electrode.

The reaction was investigated closer with a chronoamperometry experiment. The result is shown in Figure 5.6.8a. The potential was set to 3 V, and the duration of the experiment was 8 min. As seen from Figure 5.6.8b, it was observed gas evolution during the experiment. The gas development was largest the first 1-2 min and it was seen to decrease with time. On the aluminium counter, a black deposit was formed, which was most likely aluminium. It was observed that the deposit was loosely attached to the counter and when the electrode was taken out of the electrolyte, some of the deposit fell off. Most of the remaining deposit on the counter dissolved in contact with distilled water and a clean electrode surface remained.

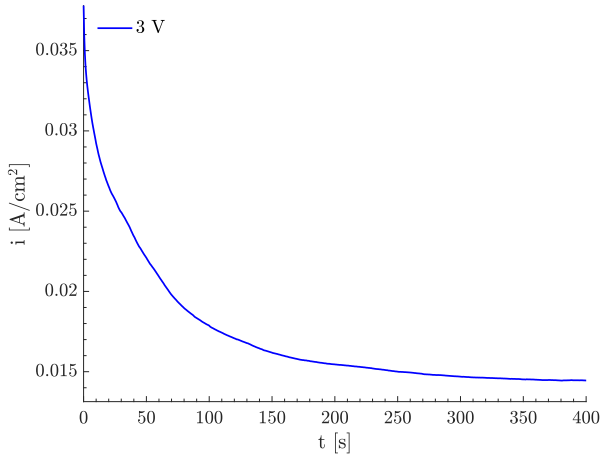

(a)

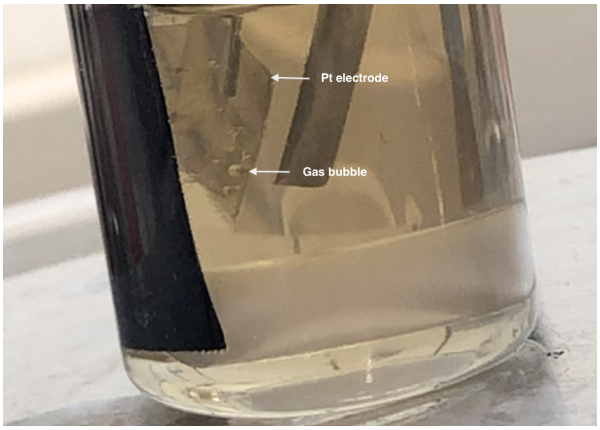

(b)

Figure 5.6.8: Chrono amperometry on Pt ($2\,cm^2$) with constant potential at 3 V (vs Al) (a) Development of current density and actual applied potential over time. (b) Gas evolution on Pt working electrode.

Rapid degradation

Separate temperature variation experiments with cyclic voltammetry were performed in a 1.5:1:0.25 melt to investigate the effect of NaCl on the electrochemical processes. The electrochemical window was therefore between $-0.3\,2\,5$V and the measurement started with cathodic polarization. The working electrode was graphite with an active area of $0.94\,\mathrm{cm}^2$ and the sweep rate was $0.1\,\mathrm{V/s}$. Figure 5.6.9 shows a cyclic voltammogram measured at $75\,^{\circ}\mathrm{C}$. At 2.3 V, the current increases rapidly. At the same time, it was observed that the graphite electrode rapidly degraded, and the temperature in the electrolyte jumped above $100\,^{\circ}\mathrm{C}$. Figure 5.6.10b shows the cell after the graphite degradation. Some particles were left in 35 % HCl, but the particles did not dissolve, indicating that they were carbon.

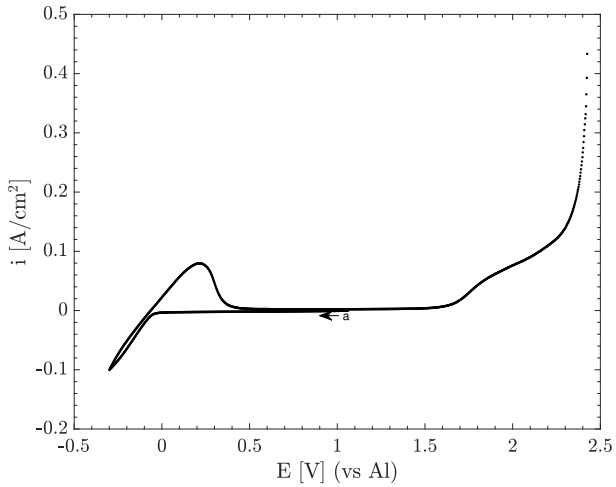

Figure 5.6.9: Cyclic voltammogram recorded in a 1.5:1:0.25 electrolyte on a $0.94\,\mathrm{cm}^2$ graphite working electrode. The sweep rate was $0.1\,\mathrm{V/s}$ and the temperature was $75\,^{\circ}\mathrm{C}$.

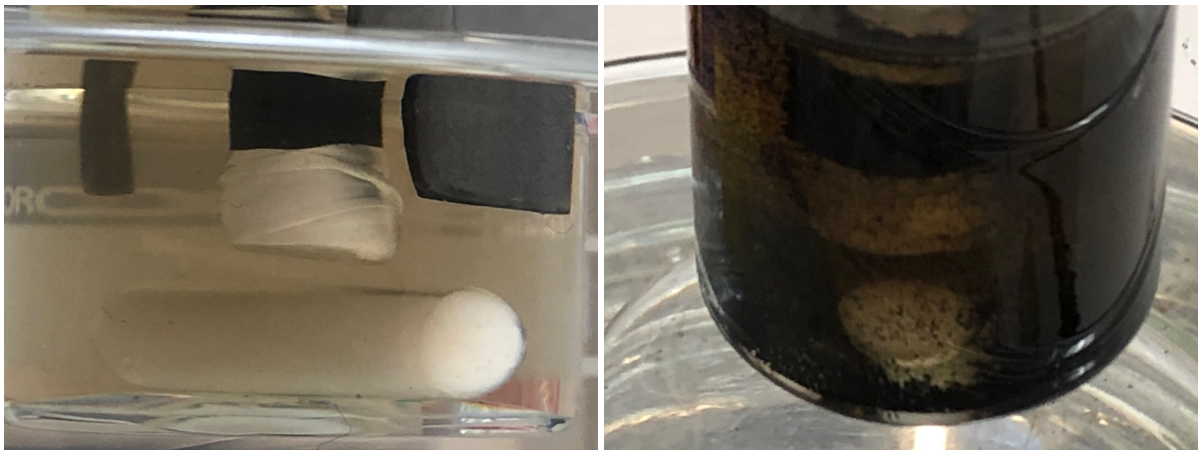

(a) **(b)**

Figure 5.6.10: (a) Cell before rapid degradation (c) cell after rapid degradation.

Figure 5.6.11 shows SEM pictures of the carbon rod before and after the degradation. It is observed that the carbon structure is pushed outwards. Figure 5.6.11c shows a picture of the graphite electrode after the degradation.

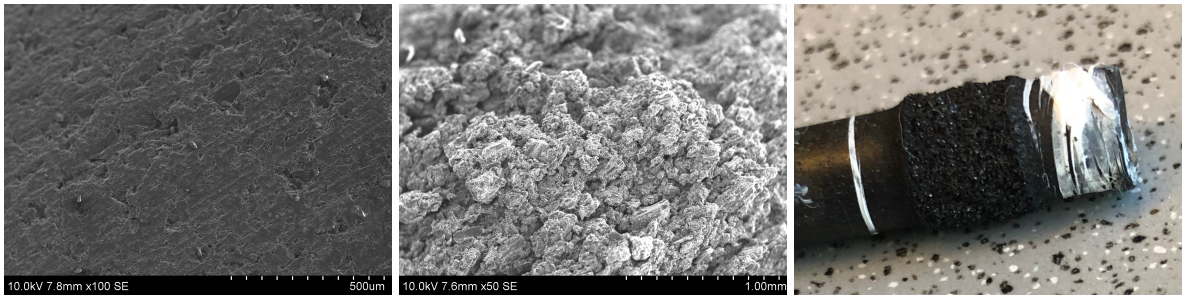

(a) Before **(b)** After **(c)** Exfoliated electrode

Figure 5.6.11: SEM pictures of the GC electrode before and after the rapid degradation, and a picture of a graphite rod.

Chapter 6

Discussion

6.1 Speciation in the $AlCl_3$-urea melt

The aim for studying the electrolytes by Raman spectroscopy was to identify the different species, their relation to the electrolyte composition and eventually use this information in the electrochemical analysis.

The chloroaluminate system is a well researched topic both in IL and ILA and the characteristic shift of $Al_2Cl_7^-$ and $AlCl_4^-$ at respectively $313\,cm^{-1}$ and $351\,cm^{-1}$ are well known and acknowledged. These shifts and other chloroaluminate shifts were found for the $AlCl_3$-urea and $AlCl_3$-urea-NaCl melts. The relative concentration of $[Al_2Cl_7^-]$ and $[AlCl_4^-]$ was dependent on the mole ratio between $AlCl_3$ and urea (Figure 5.2.2), and the results indicates that $Al_2Cl_7^-$ is present in melt where $x_{AlCl_3} > 0.5$, opposing the research of Abbott et al. [10, 14]. The peak of molecular $AlCl_3$ at $340\,cm^{-1}$ was not observed, which could support the theory of total dissociation of $AlCl_3$ into chloroaluminate species and ionic coordination complexes with urea [14]. On the other hand, it is possible that the peak of molecular $AlCl_3$ is absorbed by the strong and characteristic peak of $AlCl_4^-$.

Observation of the electrolyte reactivity towards a humid atmosphere showed a dependence on the $AlCl_3$-urea composition. The equimolar melt had the largest change over time and was almost fully crystallized after a week. The main species in this melt are $AlCl_4^-$, $[AlCl_2(urea)_2]^+$, and neutral species in the form of $AlCl_3(urea)_n$. The main contributor to the crystallization of the equimolar melt is most likely neutral species $AlCl_3(urea)_n$. $AlCl_4^-$ has a stable structure and a Lewis base. The concentration of $[AlCl_2(urea)_2]^+$ always equals the concentration of the anionic species, meaning that the sensitivity of the electrolytes should be constant or increase with $AlCl_3$, which is not the case. These species are therefore more likely to be less reactive.

These findings imply that there exists a dynamic equilibrium between the anionic, cationic and neutral species as proposed by Coleman et al. [6]. The equilibrium is shifted towards more ionic species with the addition of $AlCl_3$ according to reaction 2.2.1:

$$2AlCl_3 + 2urea \longrightarrow [AlCl_2(urea)_2]^+ + AlCl_4^-$$

and excess $AlCl_4^-$ reacts to $Al_2Cl_7^-$ through reaction 2.2.2.

$$AlCl_3 + AlCl_4^- \longrightarrow Al_2Cl_7^-$$

The concentration of both $Al_2Cl_7^-$ and $[AlCl_2(urea)_2]^+$ increases with x_{AlCl_3}. However, most likely the formation of $Al_2Cl_7^-$ is the preferred reaction as it was seen that the concentration of $AlCl_4^-$ decreased with increasing $Al_2Cl_7^-$.

With the addition of NaCl, the relative Raman intensity of $Al_2Cl_7^-$ decreased while the intensity of $AlCl_4^-$ increased. The $Al_2Cl_7^-$ peak disappears for the 1.5:1:0.5 composition, where the electrolyte was saturated with NaCl (Figure 5.2.2). This indicates that $Al_2Cl_7^-$ also participates in a Lewis acid-base equilibrium with NaCl, like the $[AlCl_2(urea)_2]^+$. It is likely that the equilibrium is similar to the one in $AlCl_3$-NaCl melts (eq. 2.5.4).

$$AlCl_4^- \longleftrightarrow Cl^- + Al_2Cl_7^-$$

6.2 Cathode processes

6.2.1 Aluminium deposition from different species in the $AlCl_3$-urea and the $AlCl_3$-urea-NaCl electrolyte

From Figure 5.5.1, aluminium deposition/stripping is seen. At a given deposition current density, the associated potential decrease with increasing $Al_2Cl_7^-/AlCl_4^-$. Relating these observations with the flat current response from the 1:1 and 1.5:1:0.5 electrolytes, where $Al_2Cl_7^-$ species is absent, it indicates that $Al_2Cl_7^-$ is the reduction complex. However, this conflicts with several papers, which suggest that only the cationic species participate in the aluminium deposition [14, 6]. Abbott et al. proposed that in equimolar melts, the potential for aluminium deposition from the cationic aluminium complex shifts to higher cathodic potential (more negative) due to changes in the electrolyte speciation [14]. Cyclic voltammetry in 1.5:1:0.25 and 1.5:1:0.35 $AlCl_3$-urea-NaCl electrolytes, showed two reduction peaks, starting at around $-0.1\,V$ and $-1.1\,V$, suggesting that the reaction in 1:1 electrolyte at higher cathodic potential and the reaction close to the reference potential (0 V) is two different reactions. Most likely the reaction at $-1.1\,V$ is aluminium deposition from $[AlCl_2(urea)_2]^+$ because the reaction was seen in 1:1 and 1.5:1:0.5 electrolytes which does not have $Al_2Cl_7^-$. This is also supported by the research of Abbott et al., who showed that the addition of LiCl to an equimolar melt decreased the deposition current. As $AlCl_4^-$ is Lewis basic, the only species LiCl might have reacted with was then $[AlCl_2(urea)_2]^+$.

The theory about two deposition reactions related to $Al_2Cl_7^-$ at around $-0.1\,V$ and $[AlCl_2(urea)_2]^+$ at around -1.1 V is further confirmed by chronoamperometry on a copper substrate in the 1.5:1:0.5 electrolyte. A dark grey product was obtained during electrolysis at $-1\,V$. Most of the deposit did not adhere to the electrode and dissolved during the cleaning. However, EDS showed aluminium oxide particles indicating that the dark grey product must have been aluminium (Figure 5.5.5b).

The implication of the theory above is that deposition from $Al_2Cl_7^-$ occurs at a less negative cathodic potential than $[AlCl_2(urea)_2]^+$ even though the latter is more Lewis acidic. Their struc-

ture might explain this. The dimeric $Al_2Cl_7^-$ species is composed of two $AlCl_4^-$ ions that share a chloride ligand bridge [54]. This structure might be weaker and more susceptible to breaking than the monomeric structure of $[AlCl_2(urea)_2]^+$ [6]. Illustrations of the suggested chemical structures are shown in Figure 6.2.1.

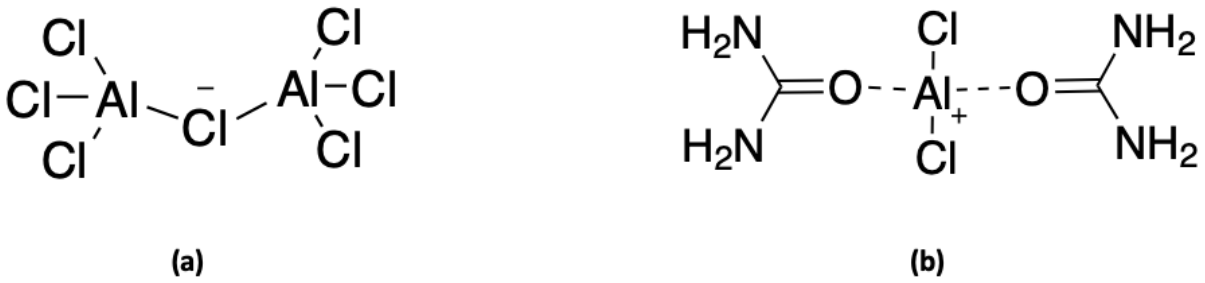

Figure 6.2.1: A suggested illustration of the chemical structures based on the work of Coleman et al., Takahashi et al., and Hvistedahl et al. [6, 54, 57]. (a) $Al_2Cl_7^-$ (b) $[AlCl_2(urea)_2]^+$.

6.2.2 Comparison of different working electrode materials

Various materials were used as working electrodes, including glassy carbon, and tungsten (Figure 5.4.1). Compared to deposition on Al, deposition on foreign materials are related to a nucleation overpotential of various magnitude. The nucleation overpotential is largest on tungsten and is about 150 mV. On glassy carbon, the nucleation overpotential is smaller, about 60 mV. Except for the nucleation overpotential, the different electrode materials gave the same current responses. This indicates that the electrode materials do not interact with the electrolyte in other reaction, making them suitable for analysis of aluminium deposition/stripping.

6.3 Factors affecting the reaction rate

Figure 5.5.1 indicates that the onset potential for aluminium deposition is shifted to more cathodic potential as the mole fraction of $Al_2Cl_7^-$ decreases. This suggests that the deposition process becomes harder when fewer electroactive species are in the melt, as predicted by the Nernst equation. It is also likely that the neutral species "dilute" the electroactive species and contribute to lower the availability of electroactive species close to the electrode. The lack of electroactive species could, therefore, affect the deposition potential. In Figure 5.5.2a, the voltammogram for the 1.3:1 electrolyte is seen to reach a current limit at -0.5 V, where the current density obtains a plateau value. This is not seen in the 1.5:1 electrolyte and could be due to a higher number of electroactive species in this electrolyte. The results from cyclic voltammetry as a function of sweep rate did not show any significant differences in the stripping current, which might indicate that the system is not dependent on mass transport.

Cyclic voltammograms recorded at various temperatures showed that the current densities increased with increasing temperature (Figure 5.5.7). This could be due to a conductivity effect because the conductivity in the melt was seen to follow an Arrhenius behaviour (Figure 5.5.8b). Based on the Hole theory, the reason for the increased conductivity could be that the voids are

larger at elevated temperatures. Also, new voids might be forming due to more frequent thermal fluctuations [58]. This results in a higher chance for the ions to find a suitable sized void to move through and hence, the conductivity increases. At the same time, the increased current density might also be due to an increase in aluminium deposition rate with the temperature. At 75 °C the characteristic current crossover found in metal deposition/stripping disappeared, indicating that the surface reaction and/or nucleation and growth processes are different at higher temperatures.

6.4 Hydrogen evolution

During cyclic voltammetry measurement to high cathodic potential, it was observed gas evolution on the working electrode (Figure 5.5.4a). Most likely, this is hydrogen evolution from urea considering that Hu et al. reported the hydrogen evolution at around $-0.8\,\mathrm{V}$ in $AlCl_3$-amide melts [7]. This might explain the broad stripping peak of 1.3:1 and 1.5:1 electrolyte in Figure 5.5.2a, which is atypical for metal stripping. The broad peak could also be due to the oxidation of various decomposed products, which were formed during the hydrogen evolution. Another possibility is that the gas formation is related to hydrogen evolution from impurities formed due to moisture. $AlCl_3$ in contact with moisture will form HCl gas, where the hydrogen ion is reducible to hydrogen gas.

6.5 Adhesion of aluminium deposits

It was observed during experiments that the aluminium deposits had poor adhesion to the working electrode, independent of the substrate. During the specialisation project, the author performed aluminium deposition in a 1.5:1 electrolyte at $-0.1\,\mathrm{V}$ on a copper substrate [56]. Compared to the electrolysis in the 1.5:1:0.5 electrolyte at $-1\,\mathrm{V}$ and also on a copper substrate, the aluminium product had a better adhesion to the substrate. This might indicate that deposition from $Al_2Cl_7^-$ gives a more continuous adherent aluminium deposit than from $[AlCl_2(urea)_2]^+$. At the same time, $[AlCl_2(urea)_2]^+$ is deposited at a potential close to the hydrogen evolution, and the contribution from the latter could also be a reason for the poor adhesion. Figure 6.5.1 shows the deposit product from the two electrolytes.

The same mechanism might occur at elevated temperatures. A cyclic voltammetry measurement at 100 °C between $-1.5\,\mathrm{V}$ and $1.3\,\mathrm{V}$ showed a dark grey deposit that did not adhere to the glassy carbon electrode (Figure 5.5.9b). Abood et al. however reported that the adhesion ability of the deposit on a copper substrate at $-0.6\,\mathrm{V}$ increased with temperature until 60 °C, showing that there is potential for aluminium deposition at higher temperatures [25].

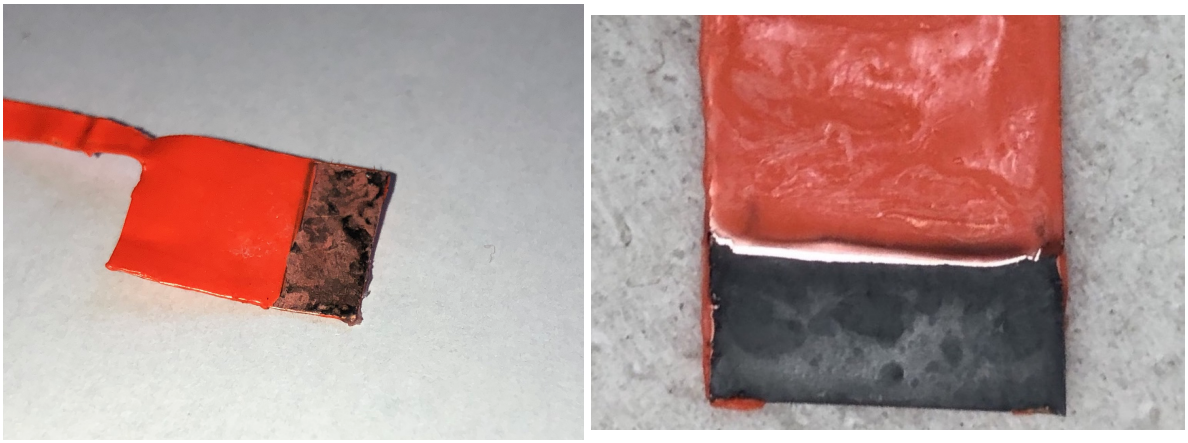

(a) (b)

Figure 6.5.1: Aluminium deposited on a copper substrate (a) in a 1.5:1:0.5 electrolyte at $-1\,\mathrm{V}$ (b) in a 1.5:1 electrolyte at $-0.1\,\mathrm{V}$. From previous work [56].

6.6 Anode processes

6.6.1 Anodic potential limit of the $AlCl_3$-urea electrolyte

The cyclic voltammogram on $1\,\mathrm{cm}^2$ aluminium showed a low current density between $2\,\mathrm{V}$ and $8\,\mathrm{V}$ (Figure 5.6.1). The current density was anodic on both the forward and reverse sweep, which could indicate that an aluminium dissolution process is occurring in this potential range. The author previously found that the capacitive current at $0.1\,\mathrm{V/s}$ was about $0.2\,\mathrm{mA/cm}^2$, which can explain the lower current density on the forward sweep (sweep towards cathodic potentials) [56]. The dissolution of the electrode occurs at a low rate, which does not change with increasing anodic potential. Most likely, the dissolution reaction is limited by the availability of free Cl ligands [9].

On the other hand, compared to the deposition and stripping current, the current flowing between $2\,\mathrm{V}$ and$8\,\mathrm{V}$ is so low that it is negligible. This could indicate that the Al substrate is passivated and the dissolution, therefore, is limited by the passivation layer. No other processes were observed in this potential window, suggesting that the electrolyte is stable in the range.

6.6.2 Chloroaluminate intercalation

Cyclic voltammetry measurements on graphite and glassy carbon in melts with and without NaCl showed a reaction starting around $1.5\,\mathrm{V}$. Based on the visible surface changes occurring to the glassy carbon electrode, and that the reaction did not occur on the metal electrodes platinum and tungsten, the reaction is most likely chloroaluminate intercalation. The onset potential is also close to the reported chloroaluminate intercalation potential by Angell et al. and Jiao et al. which was 1.6 V (vs Al) [8, 12], who also reported that the reaction is reversible, in the sense that consecutive voltammograms did not deviate from the first (Appendix A.0.1).

6.6.3 Chemically irreversible processes

A sharp rise in oxidative current density is seen for all working electrodes at around 2.3 V in both electrolytes with and without NaCl (Figures 5.6.3, 5.6.4, 5.6.7). The corresponding reaction seems to be dependent on the electrode material and electrolyte composition. For carbon electrodes, the reaction contributes to the swelling and degradation of the electrode (Figure 5.6.3). The reaction is chemically irreversible, and during the anodic polarization, the electrode is distorted and expanded. Most likely, it is the $AlCl_4^-$ species that participate in the reaction. Pan et al. reported formation of stage 3 GIC in $AlCl_3$-EMIC batteries at around 2.6 V when the temperature was $-10\,^{\circ}C$ [39]. This reaction was not observed at room temperature. Instead, an irreversible process was seen. A possible explanation for the quick degradation of the electrode, could, therefore, be that the intercalated chloroaluminates form stage 3 GIC. However, due to the higher temperature, the intercalation process occurs quicker than the coordination process, disintegrating the carbon material. Pan et al. suggested from XRD studies that the irreversible process was graphite chlorination, Cl ligands from $AlCl_4^-$ forming bonds with C on the bare surface, edges, cracks and other defects. Wang et al. also reported this phenomenon, but they concluded that this could be occurring simultaneously with the intercalation process [59]. It is therefore likely that both reactions occur on the carbon electrodes.

The process occurring on Pt and W seems to be to some degree chemically reversible as a corresponding reduction peak is observed. The onset potential for the reduction process is, however, shifted to 1.6 V and 1.9 V for W and Pt, respectively. There is not observed any gas bubbles, and the reaction can therefore not be chlorine evolution. Given that chlorine evolution from $AlCl_4^-$ has been reported in $AlCl_3$-NaCl melts, the gas reaction was expected in this melt too. Chronoamperometry experiments on Pt showed that a yellow film was formed. The film might have hindered further reaction. A closer look at the film showed that it readily reacted with the atmosphere like the electrolyte and was soluble in water. Cyclic voltammograms on Pt and W where the potential range was set to 8 V, showed that the process at 2.6 V which most likely is the film formation, eventually decreased to almost zero at around 4 V (Figure 5.6.5. The behaviour is similar to the experiment on an Al electrode. It is, however not seen any reduction corresponding to the film formation. This could indicate that the large potential window has changed the electrolyte/electrode interface before the reduction potential is reached. Above 4 V it is seen a low anodic current until 8 V, which suggests that the background process is metal dissolution. The current flow is larger on platinum. Both platinum and tungsten form compounds with chlorides. It is, therefore, reasonable to assume that the dissolution of the metals follows the same mechanism as aluminium dissolution. The voltammograms do not change much after several scans, indicating that the reaction is reproducible and is not affected by cycling. On the reverse scan, it is observed a reduction reaction after the aluminium stripping with an onset potential 0.6 V. This has not been found in any other cases and needs to be investigated further.

6.6.4 Chlorine evolution

Gas evolution was only observed for electrolytes with NaCl added. The gas formation started at around 2.3 V on platinum in an 1.5:1:0.35 electrolyte (Figure 5.6.7). According to equation 2.5.3, most of the free chlorides will form complexes with aluminium. If the gas is chlorine,

then the participating oxidation species must be $AlCl_4^-$. However, if this is the case, then chlorine evolution should also occur in electrolytes without NaCl. It is, therefore, possible that chlorine evolution occurs from free chlorides. On the other hand, chlorine evolution was only tested in 1.5:1 electrolytes, where $Al_2Cl_7^-$ was in excess ($[Al_2Cl_7^-]/[AlCl_4^-] = 1.51$). It is possible that chlorine evolution only occurs in electrolytes where $[AlCl_4^-] > [Al_2Cl_7^-]$. Chronoamperometry should, therefore, be performed on an electrolyte where the concentration of $AlCl_4^-$ is larger than $Al_2Cl_7^-$, e.g. 1.3:1 electrolyte.

Most likely the chlorine evolution also occurs on carbon materials, simultaneously with the deterioration process. This might explain the violent reactions during cyclic voltammetry measurements to 2.5 V in a 1.5:1:0.25 electrolyte at 75 °C.

6.7 Experimental errors

Several cell parameters varied from experiment to experiment related to the setup. The electrolyte resistance changed with different electrode materials and their areas, leading to a resistance difference of 3000 Ω between the largest electrode (2 cm^2) to the smallest electrode (0.01 cm^2). Comparison of working electrode showed however, that the voltammograms were quite similar after IR-corrections and the cell geometry, therefore, did not have a large impact on the processed results.

Carbon electrodes disintegrated at higher anodic potential, and the electrode surface changed drastically. It was not possible to determine the exact moment this occurred, and it is, therefore, difficult to separate the real, current response from artefacts due to area change.

It was concluded that experiments with cyclic voltammetry as a function of sweep rate in the 1.3:1 and 1.5:1 $AlCl_3$-urea did not show any sign of mass transport limitation. The cathodic peak was however, not included in the measurement. The relationship between the square root of sweep rate and current density, which might indicate if a system is mass transport limited are derived for the peak current. The relationship does, therefore, not apply to measurements where the peak current is not present. It was not possible to include the cathodic peak potential in the 1.3:1 and 1.5:1 melts because of problems with reaching this potential due to IR drop.

The prepared electrolytes were stored in the glove box. Over time it was observed changes in the electrolytes. A dark grey precipitate was observed, that could be aluminium.

Chapter 7

Conclusion

In this study, the chemical and electrochemical properties of the $AlCl_3$-urea melt have been investigated. Several electrolyte compositions with and without NaCl were prepared and investigated. Based on Raman spectroscopy, the two anionic species $AlCl_4^-$ and $Al_2Cl_7^-$ were detected in the melt. From literature review, it was found that the corresponding cation was $[AlCl_2(urea)_2]^+$.

Of the three ionic species, $Al_2Cl_7^-$ and $[AlCl_2(urea)_2]^+$ were found to be electroactive. $Al_2Cl_7^-$ was easier to reduce to aluminium ($-0.1\,V$ vs Al) than $[AlCl_2(urea)_2]^+$ ($-1.1\,V$ vs Al), even though $[AlCl_2(urea)_2]^+$ is more Lewis acidic. Based on literature data, it was believed that the monomeric coordination of $[AlCl_2(urea)_2]^+$ made it more stable than the dimeric coordination of $Al_2Cl_7^-$.

The deposition potential was dependent on the electrolyte composition. At lower $AlCl_3$ content, the deposition shifted to higher cathodic potential .

Adding NaCl reduced the cathodic current density because the salt reacted with the electroactive species. It also promoted the gas reaction which was believed to be chlorine evolution.

Without NaCl, another oxidation reaction occurred on platinum that formed a yellow film. This was not observed on tungsten due to the small electrode area. A different anode process, i.e chloroaluminate intercalation, was observed on carbon electrodes. The process was chemically reversible, but at higher anodic potential, the process lead to the disintegration of the electrode.

The main limitation of this system is the high electrolyte resistance. The specific conductivity followed an Arrhenius behaviour, and the temperature improved the current density drastically. The system showed potential to obtain current densities above $100\,mA/cm^2$.

7.1 Further work

With the current knowledge, aluminium deposition from the $AlCl_3$-urea seems to be possible, especially at elevated temperatures. There is, however, a lot of work that remains, and several problems with this melt, (i.e electrolyte resistance, deposit adhesion), that needs to be addressed before a conclusion on this matter can be made. Aluminium, in most cases, did not adhere to the electrode. Electrodeposition as function of potential, temperature and composition should

be done. The product should be examined in scanning electron microscopy and atomic force microscopy. The morphology might not be as crucial in electrowinning as in electrodeposition. However, it is still essential that the deposit adhere to the electrode.

Cyclic voltammetry experiment as a function of the sweep rate, including the aluminium deposition peak, should be done for one of the $AlCl_3$-urea-NaCl electrolytes. By doing this, a plot of peak current density vs the square root of sweep rate can be made, and information about the mass transportation in the melt can be obtained. The sweep rate experiment should also be done at 100 °C, because this can provide some information on the dependence of aluminium deposition rate on the temperature.

Two gas reactions were observed in this melt, which was believed to be hydrogen and chlorine evolution. An analysis should be done to identify the gases. The chlorine evolution is desired in an eventual electrowinning process, and methods to enhance the anode process should be investigated. It was observed that NaCl promoted the chlorine process. This could be due to an increased concentration of $AlCl_4^-$. Chlorine evolution from $AlCl_3$-urea melts with high concentration of $AlCl_4^-$ should therefore be tested. The results might provide more information about the effect of NaCl.

The cationic species have not been investigated adequately in this melt, and studies with NMR and IR-spectroscopy should be done to understand more about their interaction with the other species in solution. Their behaviour in the melt and during electrochemical measurement can give valuable information about the system which can be used in the work of optimising the process.

Bibliography

[1] Aluminium, Environment and Society. Hydro; 2012. www.hydro.com/globalassets/1-english/about-aluminium/files/aluminium_environment-and-society.pdf.

[2] Balomenos E, Panias D, Paspaliaris I, Friedrich B, Jaroni B, Steinfeld A, et al. Carbothermic reduction of alumina: A review of developed processes and novel concepts. Proceedings - European Metallurgical Conference, EMC 2011. 2011 06;3.

[3] Uchida I, Urushibata H, Toshima S. Chlorine Evolution Reaction on Tin Oxide Anodes in an AlCl 3 -NaCl Melt at 175°C. Journal of the Electrochemical Society. 1980;127(3):757–758.

[4] Zhang Q, De Oliveira Vigier K, Royer S, Jérôme F. Deep eutectic solvents: syntheses, properties and applications. RSC. 2012;41:7108–7146.

[5] Abbott A, C Barron J, Ryder K, Wilson D. Eutectic-Based Ionic Liquids with Metal-Containing Anions and Cations. Chemistry (Weinheim an der Bergstrasse, Germany). 2007 02;13:6495–501.

[6] Coleman F, Srinivasan G, Swadźba-Kwaśny M. Liquid Coordination Complexes Formed by the Heterolytic Cleavage of Metal Halides. Angewandte Chemie (International ed in English). 2013 11;52.

[7] Hu P, Zhang R, Meng X, Liu H, Xu C, Liu Z. Structural and Spectroscopic Characterizations of Amide–$AlCl_3$-Based Ionic Liquid Analogues. Inorganic Chemistry. 2016;55(5):2374–2380.

[8] Jiao H, Wang C, Tu J, Tian D, Jiao S. A rechargeable Al-ion battery: Al/molten $AlCl_3$–urea/graphite. Chem Commun. 2017;53:2331–2334.

[9] Abbott AP, Qiu F, Abood HMA, Ali MR, Ryder KS. Double layer, diluent and anode effects upon the electrodeposition of aluminium from chloroaluminate based ionic liquids. Phys Chem Chem Phys. 2010;12:1862–1872.

[10] Abood HMA, Abbott AP, Ballantyne AD, Ryder KS. Do all ionic liquids need organic cations? Characterisation of $[AlCl_2 \cdot \text{nAmide}]^+AlCl_4^-$ and comparison with imidazolium based systems. Chem Commun. 2011;47:3523–3525.

[11] Derouault J, Granger P, Forel MT. Spectroscopic investigation of aluminum trihalides-tetrahydrofuran complexes. 2. Solutions of aluminum chloride or bromide in tetrahydro-

furan and in (tetrahydrofuran-dichloromethane). Inorganic Chemistry. 1977;16(12):3214–3218.

[12] Angell M, Pan CJ, Rong Y, Yuan C, Lin MC, Hwang BJ, et al. High Coulombic efficiency aluminium-ion battery using an $AlCl_3$-urea ionic liquid analog electrolyte. PNAS. 2017;114(5):834–839.

[13] Estager J, Holbrey JD, Swadźba-Kwaśny M. Halometallate ionic liquids – revisited. Chem Soc Rev. 2014;43:847–886. Available from: http://dx.doi.org/10.1039/C3CS60310E.

[14] Abbott A, Harris R, Hsieh YT, Ryder K, Sun IW. Aluminium electrodeposition under ambient conditions. Physical chemistry chemical physics : PCCP. 2014 06;16.

[15] Pulletikurthi G, Bödecker B, Borodin A, Weidenfeller B, Endres F. Electrodeposition of Al from a 1-butylpyrrolidine-AlCl3 ionic liquid. Progress in Natural Science: Materials International. 2015;25(6):603 – 611.

[16] Fang Y, Jiang X, Sun XG, Dai S. New ionic liquids based on the complexation of dipropyl sulfide and $AlCl_3$ for electrodeposition of aluminum. Chem Commun. 2015;51:13286–13289.

[17] Gilbert B, Olivier-Bourbigou H, Favre F. Chloroaluminate Ionic Liquids: from their Structural Properties to their Applications in Process Intensification. Oil & Gas Science and Technology. 2007;62(6):745–759.

[18] Gilbert B, Chauvin Y, Guibard I. Investigation by Raman spectrometry of a new room-temperature organochloroaluminate molten salt. Analytica Chimica Acta. 1990;240(2):299–304.

[19] Li M, Gao B, Shi Z, Hu X, Wang S, Li L, et al. Electrochemical study of nickel from urea-acetamide-LiBr low-temperature molten salt. Electrochimica Acta. 2015;169:82 – 89.

[20] Li M, Gao B, Chen W, Liu C, Wang Z, Shi Z, et al. Electrodeposition behavior of aluminum from urea-acetamide-lithium halide low-temperature molten salts. Electrochimica Acta. 2015;185:148 – 155.

[21] Abbott AP. Application of Hole Theory to the Viscosity of Ionic and Molecular Liquids. Chem Phys Chem. 2004;5:1242–1246.

[22] Hu P, Jiang W, Zhong L, Zhou S. Physicochemical properties of amide–AlCl3 based ionic liquid analogues and their mixtures with copper salt. Chinese Journal of Chemical Engineering. 2019;27(1):144 – 149.

[23] Liu C, Chen W, Wu Z, Gao B, Hu X, Shi Z, et al. Density, viscosity and electrical conductivity of AlCl3-amide ionic liquid analogues. Journal of Molecular Liquids. 2017;247:57–63.

[24] Jeffrey GA. An introduction to hydrogen bonding. New York: Oxford University Press; 1997.

[25] A Hadi M, Abood H, L Dawood N. Morphology of Electrodeposited Aluminium Metal from Aluminium Chloride-Urea Room Temperature Ionic Liquid (RTIL) at Variable Parameters. International Journal of Science and Research (IJSR). 2015 09;4:4–438.

[26] Samikannu P, Wang HW. Factors Affecting the Electrodeposition of Aluminum Metal in an Aluminum Chloride–Urea Electrolyte Solution. Journal of the Chinese Chemical Society. 2017 11;64.

[27] Stafford GR, Haarberg GM. The electrodeposition of Al-Nb alloys from chloroaluminate electrolytes. Plasmas & Ions. 1999;2(1):35–44.

[28] Cotton SA. Chemistry of precious metals. London: Blackie Academic & Professional; 1997.

[29] Inorganic syntheses. : Volume 36. Hoboken, New Jersey; 2014.

[30] Boxall LG, Jones HL, Osteryoung RA. Solvent Equilibria of $AlCl_3$-NaCl Melts. J Electrochem Soc. 1973;120.

[31] Chemistry of Nonaqueous Solutions: Current Progress (Mamantov, Gleb; Popov, Alexander I.). Journal of Chemical Education. 1995;72(3).

[32] Abood H, Fadhil M. Investigation of Lewis Acid-Base Reaction of Acidic Species Present in Aluminum Chloride-Urea Ionic Liquid [AlCl2.nUrea] +. Journal of Al-Nahrain University. 2014 03;17:71–75.

[33] Sun H, Wang W, Yu Z, Yuan Y, Wang S, Jiao S. A new aluminium-ion battery with high voltage, high safety and low cost. Chem Commun. 2015;51:11892–11895.

[34] Lin MC, Gong M, Lu B, Wu Y, Wang DY, Guan M, et al. An ultrafast rechargeable aluminium-ion battery. Nature. 2015;520(7547).

[35] Mohandas K, Sanil N, Noel M, Rodriguez P. Anodic behaviour of carbon materials in NaCl saturated $NaAlCl_4$ fused electrolyte at low temperatures: A cyclic voltammetric study. Journal Of Applied Electrochemistry. 2001;31(9):997–1007.

[36] Urushibata H, Uchida I, Toshima S. The kinetics of chlorine evolution and reduction on glassy carbon in molten tetrachloroaluminate at 175°C. Journal of Electroanalytical Chemistry. 1981;117(1):43–52.

[37] Holleck GL. The Reduction of Chlorine on Carbon in AlCl 3 -KCI-NaCI Melts. Journal of the Electrochemical Society. 1972;119(9):1158–1161.

[38] Schmuelling G, Placke T, Kloepsch R, Fromm O, Meyer HW, Passerini S, et al. X-ray diffraction studies of the electrochemical intercalation of bis(trifluoromethanesulfonyl)imide anions into graphite for dual-ion cells. Journal of Power Sources. 2013;239:563 – 571.

[39] Pan CJ, Yuan C, Zhu G, Zhang Q, Huang CJ, Lin MC, et al. An operando X-ray diffraction study of chloroaluminate anion-graphite intercalation in aluminum batteries. Proceedings of the National Academy of Sciences. 2018;115(22).

[40] Borg RJ. An introduction to solid state diffusion. Boston: Academic Press; 1988.

[41] Dzurus ML, Hennig GR. Graphite Compounds. Journal of the American Chemical Society. 1957;79(5):1051–1054.

[42] Robinson J, Osteryoung RA. An investigation into the electrochemical oxidation of some aromatic amines in the room-temperature molten salt system aluminum chloride-butylpyridinium chloride. Journal of the American Chemical Society. 1980;102(13):4415–4420.

[43] Jiang T, J Chollier Brym M, Dubé G, Lasia A, Brisard GM. Electrodeposition of aluminium from ionic liquids: Part I—electrodeposition and surface morphology of aluminium from aluminium chloride ($AlCl_3$)–1-ethyl-3-methylimidazolium chloride ([EMIm]Cl) ionic liquids. Surface and Coatings Technology. 2006 09;201:1–9.

[44] Carlin RT. Nucleation and Morphology Studies of Aluminum Deposited from an Ambient-Temperature Chloroaluminate Molten Salt. Journal of The Electrochemical Society. 1992;139(10).

[45] Instrumental methods in electrochemistry. Repr. with corrections. ed. Ellis Horwood series in physical chemistry. New York: Ellis Horwood; 1990.

[46] Fisher AC. Electrode dynamics. vol. 34 of Oxford chemistry primers. Oxford: Oxford University Press; 1996.

[47] Hamann CH. Electrochemistry. 2nd ed. Weinheim: Wiley; 2007.

[48] Kim JY, Suk Choi Y, Bae SE, Yum I, Hyeon Kim D, Yeon JW, et al. Electrical Conductivity Measurement of Molten Salts Using a Two-Electrode Alternative Current Impedance Method. Asian Journal of Chemistry. 2013 09;25:7028–7030.

[49] T Niitsu G, Nagata H, Rodrigues ACM. Electrical properties along the X and Z axes of LiNbO3 wafers. Journal of Applied Physics. 2004 03;95:3116–3119.

[50] Raman Spectroscopy basics - Application note. Princeton Instruments; 2011. http://web.pdx.edu/~larosaa/Applied_Optics_464-564/Projects_Optics/Raman_Spectrocopy/Raman_Spectroscopy_Basics_PRINCETON-INSTRUMENTS.pdf.

[51] Jarle H. Detectors in SEM; 2000. University Lecture in TMT4166.

[52] Frost RL, Kristof J, Rintoul L, Kloprogge JT. Raman spectroscopy of urea and urea-intercalated kaolinites at 77 K. Spectrochimica Acta Part A: Molecular and Biomolecular Spectroscopy. 2000;56(9):1681 – 1691. Available from: http://www.sciencedirect.com/science/article/pii/S1386142500002237.

[53] Ferraro JR, Ziomek JS, Mack G. Raman spectra of solids. Spectrochimica Acta. 1961;17(8):802 – 814.

[54] Takahashi S, Curtiss LA, Gosztola D, Koura N, Saboungi ML. Molecular Orbital Calculations and Raman Measurements for 1-Ethyl-3-methylimidazolium Chloroaluminates. Inorganic Chemistry. 1995;34(11):2990–2993.

[55] Gale RJ, Gilbert B, Osteryoung RA. Raman spectra of molten aluminum chloride: 1-butylpyridinium chloride systems at ambient temperatures. Inorganic Chemistry. 1978;17(10):2728–2729.

[56] Nguyen T. Aluminium deposition from an $AlCl_3$-Urea electrolyte [Specialization project]. 2018;.

[57] Hvistendahl J, Klaeboe P, Rytter E, Oeye HA. Infrared emission spectra of alkali chloroaluminates and related melts. Inorganic Chemistry. 1984;23(6):706–715.

[58] Gibbs JW. Elementary principles in statistical mechanics : developed with especial reference to the rational foundation of thermodynamics J. Willard Gibbs. Woodbridge, CT: Ox Bow Press; 1981.

[59] Wang DY, Wei CY, Lin MC, Pan CJ, Chou HL, Chen HA, et al. Advanced rechargeable aluminium ion battery with a high-quality natural graphite cathode. Nature Communications. 2017;8.

[60] Bale CW, Bélisle E, Chartrand P, Decterov SA, Eriksson G, Gheribi AE, et al.. FactSage Thermochemical Software and Databases; 2010-2016. `www.factsage.com`.

Appendices

Appendix A

Cyclic voltammograms

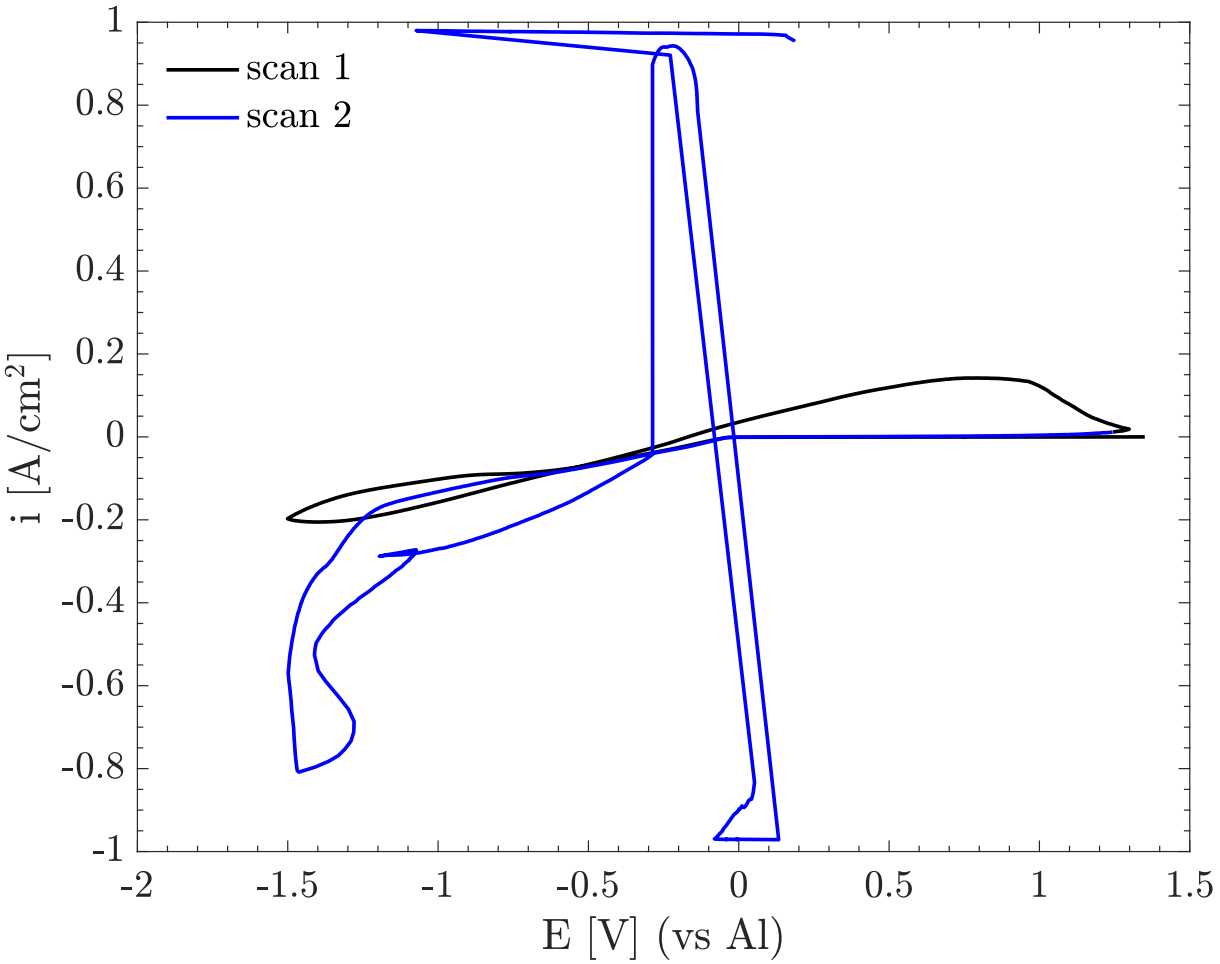

Figure A.0.1: Cyclic voltammetry in a 1.5:1 electrolyte at 100 °C. Two consecutive sweep are shown for the voltammogram in Figure 5.5.8. The sweep rate was 0.1 V/s and the working electrode was glassy carbon with an area of 0.2 cm^2.

[h]

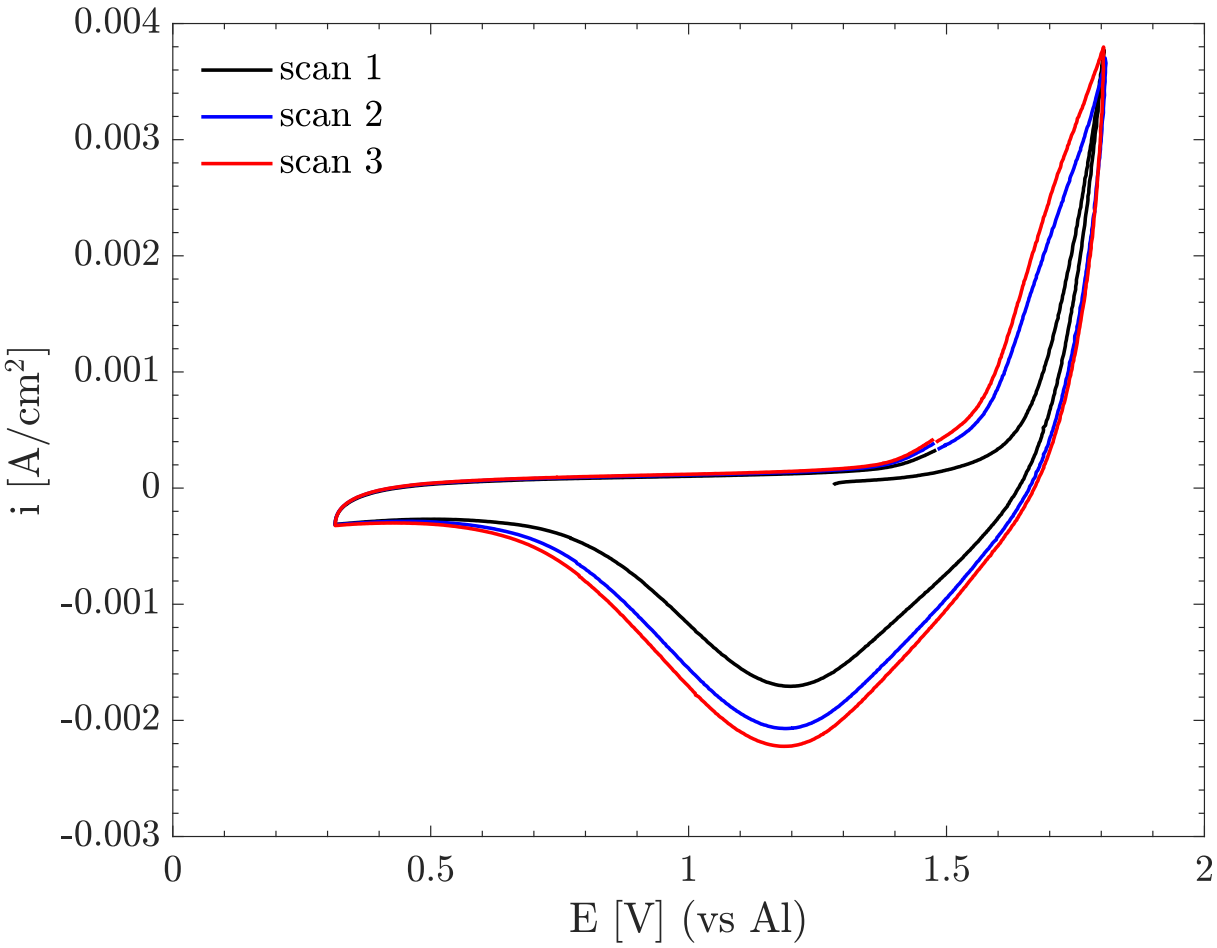

Figure A.0.2: Cyclic voltammogram in a 1.5:1 electrolyte. The working electrode was a 0.2 cm^2 glassy carbon and the sweep rate was $-0.1\,\mathrm{V/s}$. Consecutive scans of the voltammogram in Figure 5.6.2a

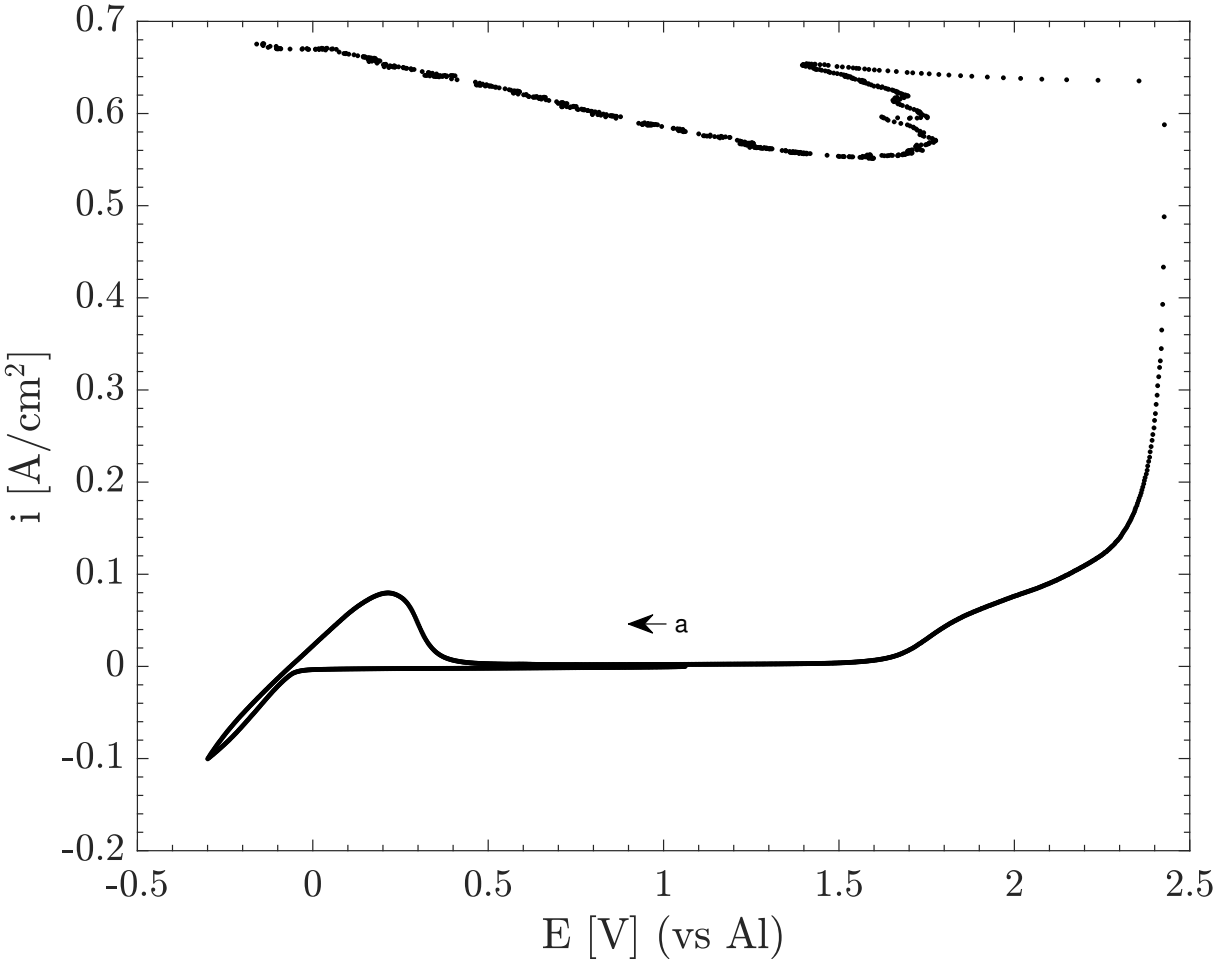

Figure A.0.3: Cyclic voltammogram in a 1.5:1:0.5 electrolyte showing the current response after the electrode quickly degraded in Figure 5.6.9. The working electrode was graphite with an area of $0.94\,\mathrm{cm}^2$ and the sweep rate was $-0.1\,\mathrm{V/s}$.

Appendix B

Phase diagrams

The phase diagrams were taken from Factsage [60]-.

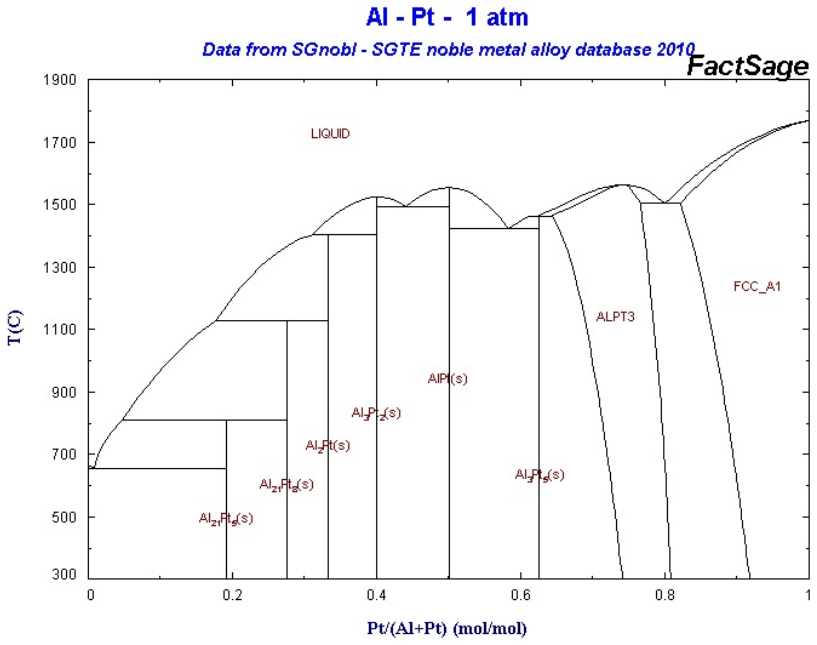

Figure B.0.1: Phase diagram for the Al-Pt system [60]

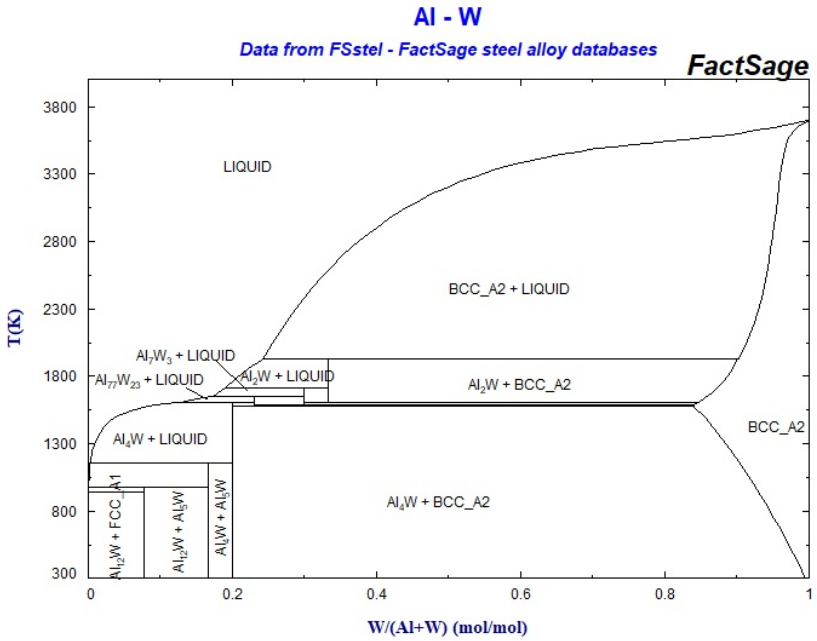

Figure B.0.2: Phase diagram for the Al-W system [60]

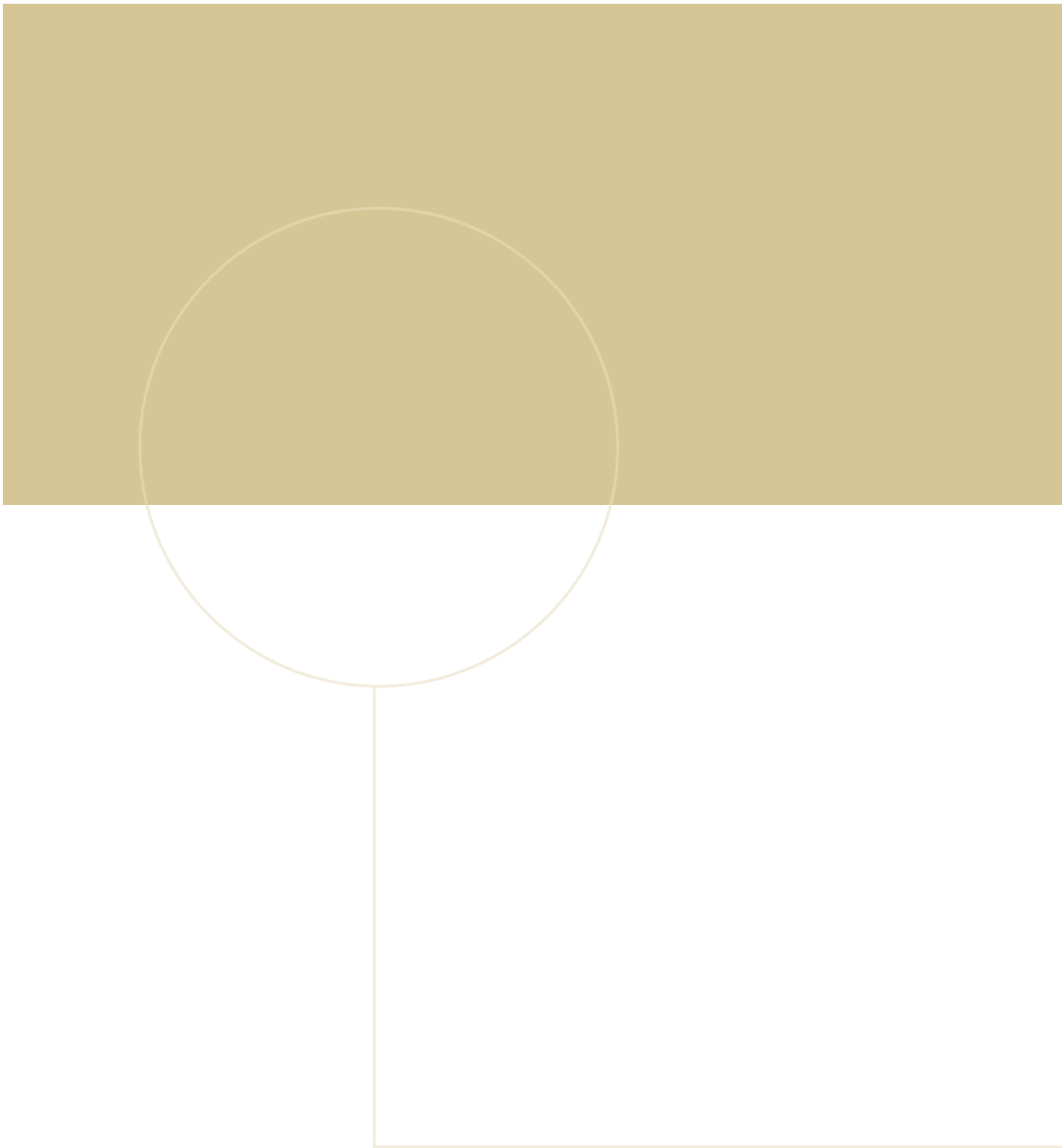

NTNU
Norwegian University of
Science and Technology